Flat Slabs in Eccentric Punching Shear: Experimental Database and Code Analysis

Vargas, Daniel ; Lantsoght, E.O.L.; Genikomsou, Aikaterini S.

Important note
To cite this publication, please use the final published version (if applicable).
Please check the document version above.

Flat Slabs in Eccentric Punching Shear: Experimental Database and Code Analysis

Daniel Vargas [1], Eva O. L. Lantsoght [1,2,*] and Aikaterini S. Genikomsou [3]

1   Politécnico, Universidad San Francisco de Quito, Quito 170901, Ecuador
2   Concrete Structures, Department of Engineering Structures, Civil Engineering and Geosciences, Delft University of Technology, 2628 CD Delft, The Netherlands
3   Faculty of Engineering and Applied Science—Civil Engineering, Queen's University, Kingston, ON K7L 3N6, Canada
*   Correspondence: e.o.l.lantsoght@tudelft.nl

Abstract: Eccentric punching shear can occur in concrete slab–column connections when the connection is subjected to shear and unbalanced moments. Unbalanced moments occur in all floor slabs at the edge and corner columns. As such, this problem is of practical relevance. However, most punching experiments in the literature deal with concentric punching shear at internal columns. This paper presents a developed database of 128 experiments of flat slabs under eccentric punching shear, including a summary of the testing procedure of each reference and a description of the slab specimens. Additionally, a linear finite element analysis of all the specimens is included to determine the relevant sectional shear forces and moments. Finally, the ultimate shear stresses from the database experiments are compared to the shear capacities determined with ACI 318-19, Eurocode 2 and the Model Code 2010. The comparison shows that the Model Code 2010 is the most precise in the predictions with an average tested to predicted ratio of 0.82 and a coefficient of variation of 29.63%. It can be concluded that improvements to the current design methods for eccentric punching shear are necessary.

Keywords: code provisions; database; eccentric punching shear; experiments; flat slab; linear finite element models; punching; reinforced concrete; shear; unbalanced moments

1. Introduction

Reinforced concrete flat slab floor systems are an interesting solution for building design due to the simplicity of the construction process, story height reduction in comparison to systems with beams and the associated economic advantages. Nevertheless, a difficulty lies in predicting the slab–column connection behavior and capacity when lateral loads or unbalanced gravity loads cause the transfer of moments between the slab and the column [1], as occurs at the edge and corner columns. Unbalanced moments can also be caused by asymmetrical spans, creep and differential shrinkage between two continuous slabs [2].

A few collapses caused by punching failure have been reported throughout the years, which gained the attention of researchers and practitioners [3]. One example is the collapse of the underground parking garage in Gretzenbach, Switzerland, in November 2005 [4]. The collapsed structure had no shear reinforcement; only column capitals were provided for shear enhancement. This collapse caused the deaths of seven people.

Typically, the most critical slab–column connections are located at the corners and edges, as these connections are subjected to moment transfer and eccentric loading. However, these cases are less studied experimentally in comparison with internal slab–column connections under concentric loads. The vast majority of experiments are carried out on slab–column connections with concentric loading.

The first comprehensive studies on punching shear were performed in the 1960s by Kinnunen and Nylander [5], but their mechanical models resulted in complicated expressions, which code makers found impractical for use [6]. Instead, empirical expressions based on the available test results were created for the development of the code provisions. Given that there is a lack of experimental information on eccentric punching shear on large-scale flat slabs, it became difficult to provide a satisfactory design expression [2]. To account for the eccentric loading, ACI 318-19, Eurocode 2 EN 1992-1-1:2005 and the *fib* Model Code 2010 models considered the shear stress distribution on the critical perimeter [7–9], assuming either a linear or plastic stress distribution. The punching perimeter is at a distance $d/2$ from the column in ACI 318-19, and it is at the same distance, but with rounded corners, in the *fib* Model Code 2010. Eurocode 2 uses a perimeter at a distance $2d$ from the column, and the perimeter has rounded corners as well.

Despite the efforts undertaken by investigators through the years, the current design methods cannot accurately predict the punching shear strengths when unbalanced moments act on slabs. Nowadays, the advances in materials and new analysis methodologies, such as nonlinear finite element analysis and better instrumentation techniques for experimental campaigns, have helped researchers start proposing a reshaping of the design codes to best meet the real performance of the slab–column connections under eccentric loading [10].

This work aims to present a wider view of the problem by compiling and analyzing experiments on eccentric punching shear from the literature. The analysis of the compiled experiments can be used to examine the performance of the currently available building codes and identify which types of experiments would be a valuable contribution to the body of knowledge. Additional experiments could be used to refine and improve the existing models. In addition, the developed database can serve those who are working on mechanical models of punching shear to check the performance for the case of eccentric punching.

This article compiles 128 experiments on flat slabs in eccentric punching shear. Vertical, horizontal and combined loading setups are reported in the literature. Both slabs with and without shear reinforcement are included in the developed database. The internal forces of the slabs for the maximum applied load, i.e., at the onset of punching shear failure, are typically not available in the references. To complete the missing information, a linear finite element model of each experiment is constructed. The experimental shear capacities from the database are then compared to the strengths predicted by the design expressions found in ACI 318-19 [7], Eurocode 2 NEN-EN 1992-1-1:2005 [8] and the *fib* Model Code 2010 [9].

2. Methods

2.1. Overview of Code Provisions

2.1.1. ACI-318-19

The punching shear provisions from ACI 318-19 are based on empirical equations derived from test results by Moe [11] and analyses by the ACI-ASCE Committee 426 [12]. The ACI 318-19 method is based on the maximum shear stress v_u on the critical perimeter b_o of the slab, which is located at $0.5\,d$ from the face of the column, where d is the average slab effective depth. The maximum shear stress v_u should not exceed the nominal shear strength of the slab v_n. Figure 1 is a sketch of the shear stresses produced by axial load and moment transfer on an internal slab–column connection [1].

Shear stresses due to $Y_v (M_{u1} - M_{u2})$

(a)

$$v = \frac{V_u}{b_o\, d}$$

(b)

$$v = \frac{Y_v (M_{u1} - M_{u2})\, c}{J_c}$$

(c)

(d)
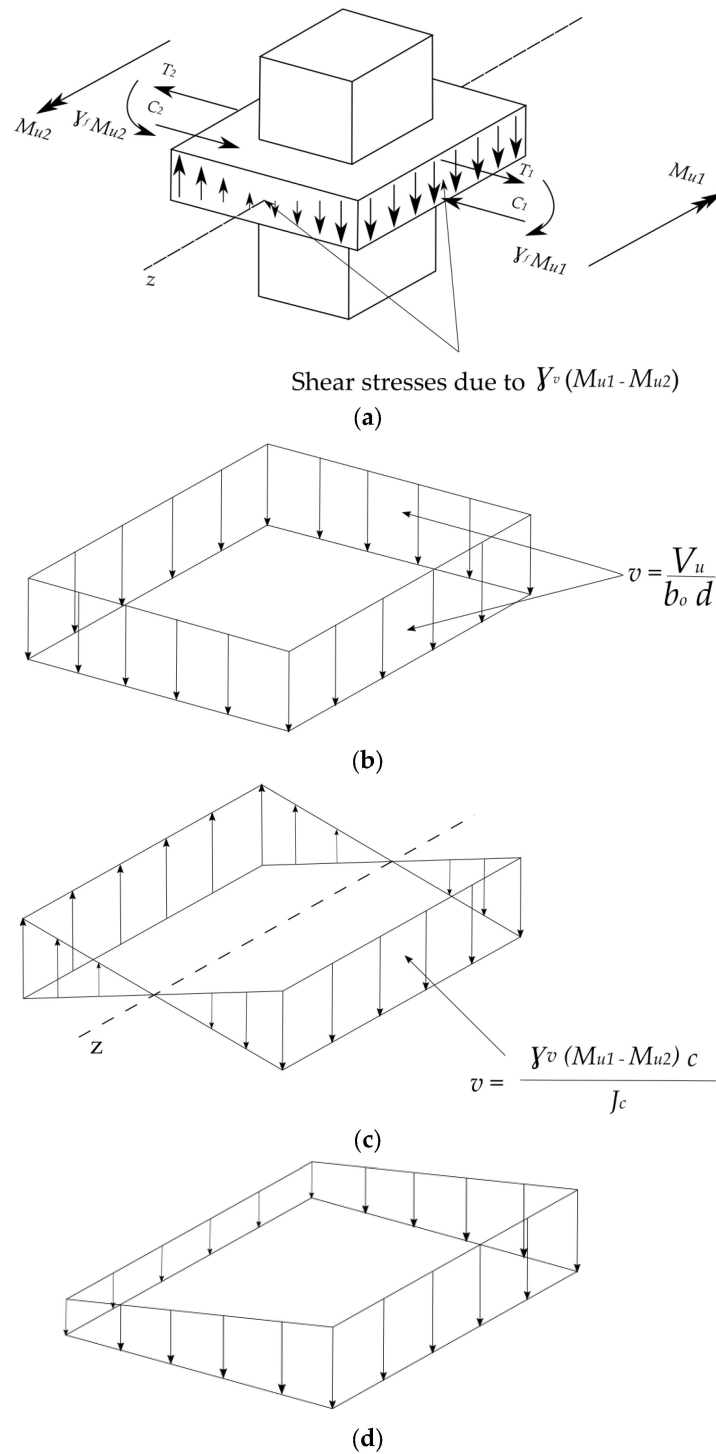
Figure 1. Shear stress produced by applied load and moment transfer, modified from Ref. [1]: (**a**) transfer of unbalanced moments to column; (**b**) shear stress caused by direct shear; (**c**) shear stress caused by unbalanced moments; (**d**) total shear stress: sum of (**b**,**c**).

MacGregor and Wight [1] define v_u using the following equation:

$$v_u = \frac{V_u}{b_o d} \pm \frac{\gamma_v M_u c}{J_c} \tag{1}$$

where V_u is the factored shear being transferred from the slab to the column acting on the centroid of the critical section; c is the distance from the centroid of the critical section to

the point where the shear stress is calculated; J_c is the polar moment of inertia of the critical section; and $\gamma_v M_u$ is the fraction of moment transferred by the shear, with γ_v as follows:

$$\gamma_v = 1 - \gamma_f \tag{2}$$

where γ_f is the fraction of moment transmitted by flexure

$$\gamma_f = \frac{1}{1 + \left(\frac{2}{3}\right)\sqrt{\frac{b_1}{b_2}}} \tag{3}$$

where b_1 is the total width of the critical section measured perpendicular to the axis around which the moment acts, and b_2 is the total width parallel to the axis [1]. Figure 2 shows a sketch of the critical perimeter of an interior, edge and corner slab–column connection.

(a)

(b)

(c)
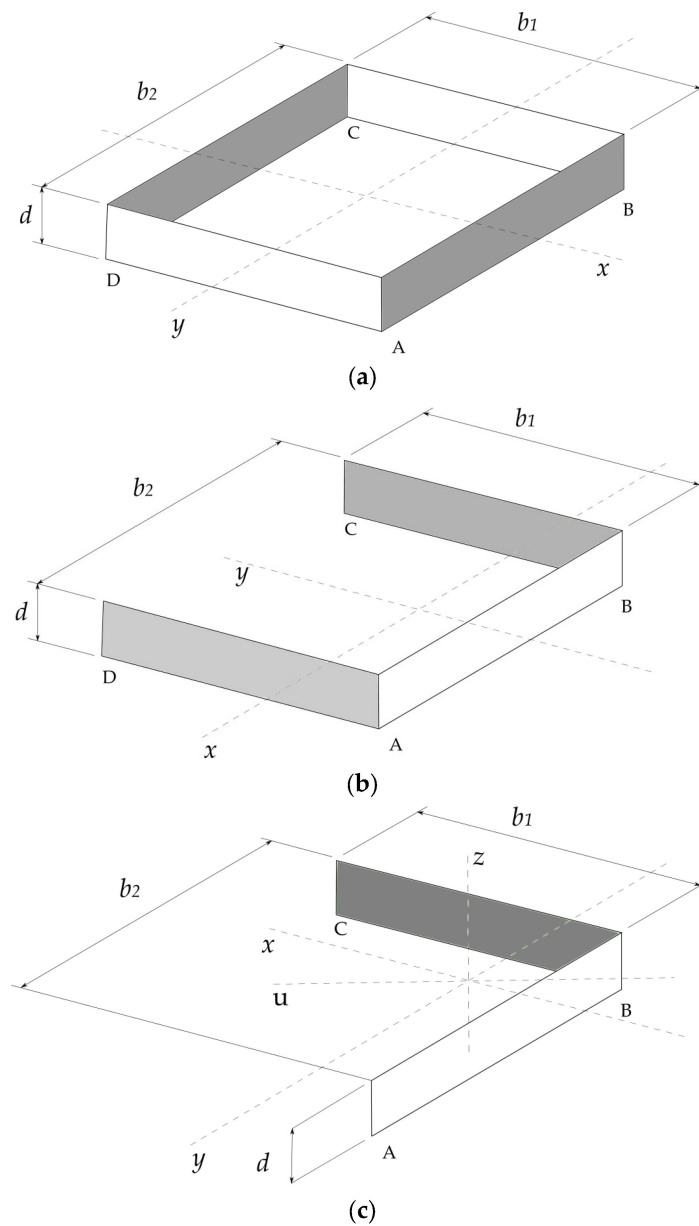
Figure 2. Critical perimeter of an interior, edge and corner slab–column connections, modified from Ref. [1]: (**a**) interior slab–column connection; (**b**) edge slab–column connection; (**c**) corner slab–column connection.

The ultimate shear capacity v_n is calculated as follows, with v_u as determined by Equation (1):

$$v_n = v_c + v_s \geq v_u \tag{4}$$

According to ACI 318-19 Section 22.6.5.2, in slabs without reinforcement, the shear stress shall not exceed the least of the following three expressions, with f'_c in [MPa] [7]:

$$v_c = 0.33 \lambda_s \lambda \sqrt{f'_c} \tag{5}$$

$$v_c = 0.17 \left(1 + \frac{2}{\beta} \right) \lambda_s \lambda \sqrt{f'_c} \tag{6}$$

$$v_c = 0.083 \left(2 + \frac{\alpha_s d}{b_o} \right) \lambda_s \lambda \sqrt{f'_c} \tag{7}$$

The value of α_s is 40 for interior columns, 30 for edge columns and 20 for corner columns; λ_s is the size effect modification factor; λ is the lightweight factor; and β is the ratio of long to short column sizes [7].

The contribution of the shear reinforcement v_s is determined as

$$v_s = \frac{A_v f_{yt}}{b_o s} \tag{8}$$

where A_v is the sum of the area of all legs of reinforcement on the peripheral line, which is geometrically like the perimeter of the column section; f_{yt} is the yield strength of the transverse reinforcement; and s is the spacing of transversal reinforcement [7].

Section 22.6.6.1 [7] indicates that the value of v_c for shear-reinforced slabs shall not exceed the following:

$$v_c = 0.17 \lambda_s \lambda \sqrt{f'_c} \tag{9}$$

$$v_c = 0.25 \lambda_s \lambda \sqrt{f'_c} \tag{10}$$

$$v_c = \left(0.17 + \frac{0.33}{\beta} \right) \lambda_s \lambda \sqrt{f'_c} \tag{11}$$

$$v_c = \left(0.17 + \frac{0.083 \alpha_s d}{b_o} \right) \lambda_s \lambda \sqrt{f'_c} \tag{12}$$

Equation (9) is used for stirrup reinforcement, and Equations (10)–(12) are used for headed shear stud reinforcement, where the least of them shall be taken. When shear reinforcement is used, the critical perimeter b_o shall be taken outside the reinforced section, as illustrated in Figure 3 [7].

2.1.2. NEN-EN 1992-1-1:2005

The punching shear provisions of NEN-EN 1992-1-1:2005 contain empirical equations for concrete contribution to the two-way shear capacity, based on the elastic analysis performed by Mast [13]. It is assumed that the concrete contribution to the shear capacity in terms of shear stresses is equal for one-way shear (beam shear) and two-way shear (punching shear), although for two-way shear, the reinforcement ratio is taken as the geometric average of both reinforcement directions, whereas for one-way shear, only the reinforcement ratio of longitudinal reinforcement is considered.

According to the provisions of NEN-EN 1992-1-1:2005, the punching shear is checked at the face of the column and at the basic control perimeter U_1 [8]. The basic control perimeter U_1 is located at $2d$ from the loaded area, with d as the average effective depth of the slab. Figure 4 shows the basic control perimeter for an interior, edge and corner slab–column connection [8]. Note that rounded corners are used for the perimeter.
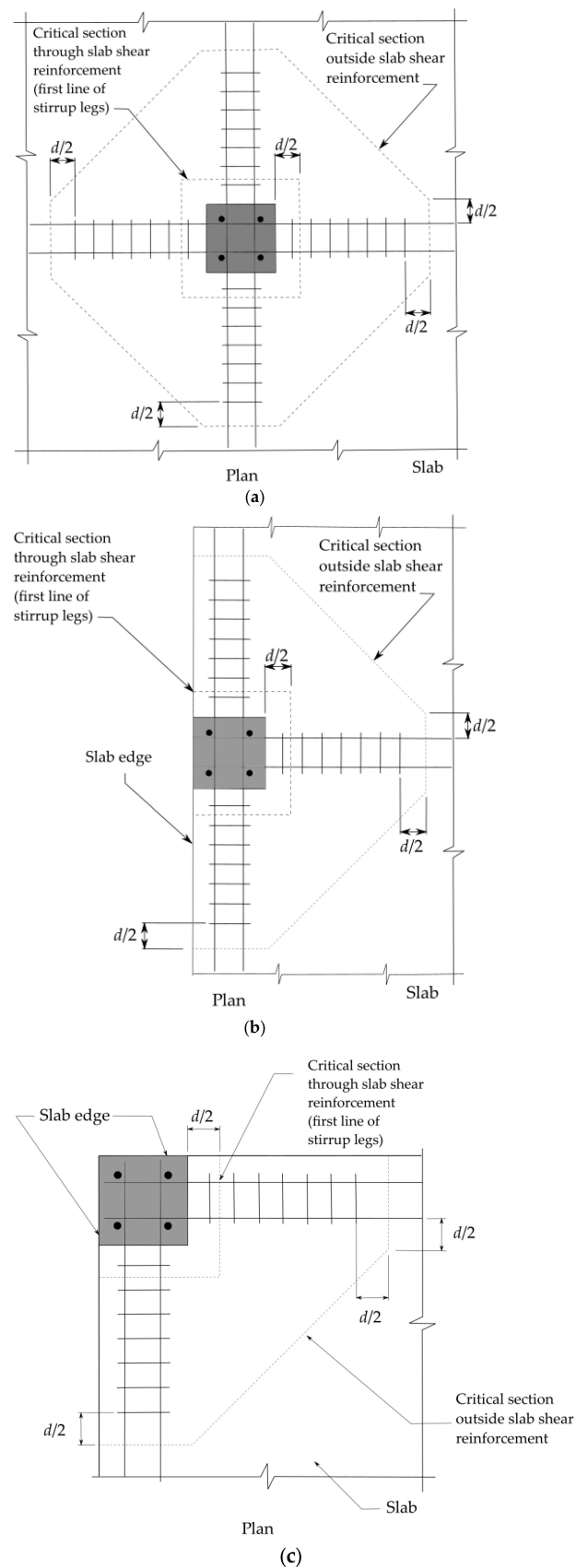
Figure 3. Critical perimeter for a shear-reinforced interior, edge and corner slab–column connection, modified from Ref. [7]: (**a**) interior slab–column connection; (**b**) edge slab–column connection; (**c**) corner slab–column connection.
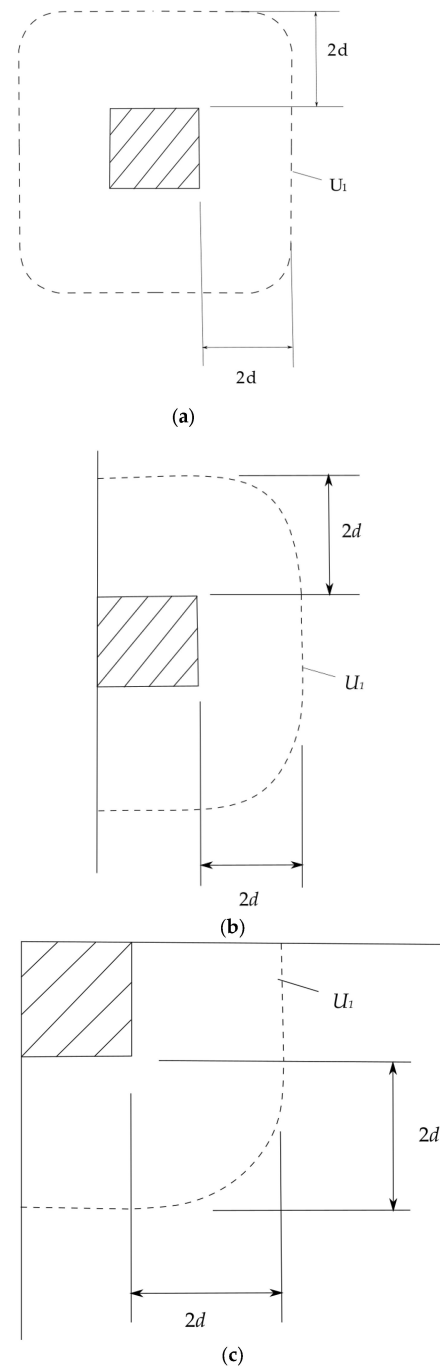
Figure 4. Basic control perimeter for an interior, edge and corner slab–column connection, modified from Ref. [8]: (**a**) interior slab–column connection; (**b**) edge slab–column connection; (**c**) corner slab–column connection.

Punching shear is evaluated based on the following stresses: $v_{Rd,c}$—the design value of the punching shear resistance of a slab without punching shear reinforcement; $v_{Rd,s}$—the value of the punching shear resistance of a slab with punching shear reinforcement; and v_{Ed}—the maximum acting shear stress along the control section. If $v_{Ed} \leq v_{Rd,c}$, then punching shear reinforcement is not necessary. If the support reaction is eccentric with respect to the control perimeter, the maximum shear stress is

$$v_{Ed} = \beta_{EC} \frac{V_{Ed}}{U_1 d} \tag{13}$$

$$\beta_{EC} = 1 + k_c \frac{M_{Ed}}{V_{Ed}} \frac{U_1}{W_1} \qquad (14)$$

where W_1 represents the shear distribution on the control perimeter; V_{Ed} is the design value of the sectional shear force; M_{Ed} is the design value of the sectional bending moment; and k_c is a coefficient on the ratio between the column dimensions given by Table 6.1 of NEN-EN 1992-1-1:2005 [8]. A few values of k_c are 0.6 for a c_1/c_2 ratio of 1.0 and 0.70 for a c_1/c_2 ratio of 2.0, where c_1 and c_2 are the dimensions of the column (see Figure 5). W_1 is calculated as

$$W_1 = \int_0^{U_i} |e| dl \qquad (15)$$

where U_i is the length of the control perimeter under consideration; dl is a length increment of the perimeter; and e is the distance of dl from the axis around which the moment M_{Ed} acts [8]. Figure 5 shows shear distribution due to an unbalanced moment at a slab–column connection, indicating that the Eurocode approach assumes a fully plastic distribution of the shear stresses.
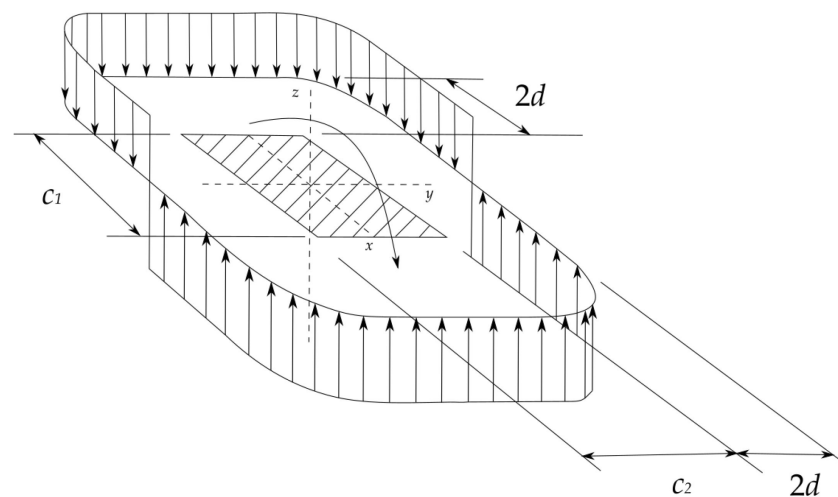
Figure 5. Shear distribution due to an unbalanced moment at a slab–column connection, modified from Ref. [8].

For an internal rectangular column where the loading is eccentric to both orthogonal axes, β_{EC} shall be calculated as follows:

$$\beta_{EC} = 1 + 1.8 \sqrt{\left(\frac{e_y}{b_x}\right)^2 + \left(\frac{e_x}{b_y}\right)^2} \qquad (16)$$

where e_y and e_x are the eccentricities M_{Ed}/V_{Ed} along the axes y and x, respectively, and b_x and b_y are the dimensions of the control perimeter. For edge slab–column connections, where the eccentricity is perpendicular to the slab edge toward the interior, and there is no eccentricity parallel to the edge, the control perimeter may be reduced to $U_1{}^*$, as illustrated in Figure 6a. For corner slab–column connections, where the eccentricity is toward the interior of the slab, the control perimeter may be reduced to $U_1{}^*$, as illustrated in Figure 6b [8]. This approach was adopted for safety reasons, considering that when there is a moment around an axis parallel to the slab edge or a moment at a corner column, the experimental results showed that punching failure is typically preceded by torsional cracking at the edge of the slab [14].
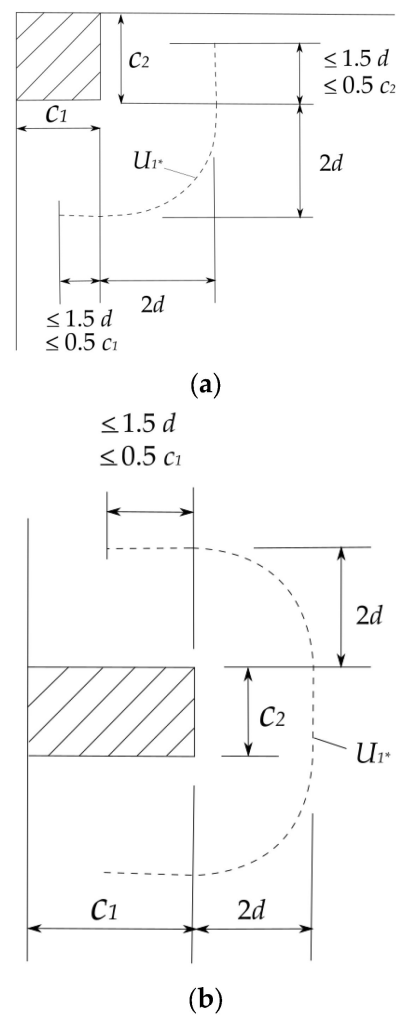
Figure 6. Reduced basic control perimeter, modified from Ref. [8]: (**a**) edge slab–column connection; (**b**) corner slab–column connection.

For edge slab–column connections, if there are eccentricities in both orthogonal directions, β_{EC} shall be calculated as

$$\beta_{EC} = \frac{U_1}{U_1^*} + k_c \frac{U_1}{W_1} e_{par} \tag{17}$$

where e_{par} is the eccentricity parallel to the slab edge. For edge and corner column connections, where the eccentricity is toward the interior of the slab, β_{EC} shall be calculated as

$$\beta_{EC} = \frac{U_1}{U_1^*} \tag{18}$$

If the eccentricity is toward the exterior, β_{EC} shall be calculated using Equation (16).

The punching shear resistance of slabs without shear reinforcement $v_{Rd,c}$ is calculated as

$$v_{Rd,c} = C_{Rd,c} k (100\rho_l f_{ck})^{\frac{1}{3}} \geq v_{min} \tag{19}$$

with $v_{Rd,c}$ taken as $0.18/\gamma_c$, with γ_c the material factor for concrete ($\gamma_c = 1.5$) and k the size effect factor, calculated with the following expression, with d in [mm]

$$k = 1 + \sqrt{\frac{200}{d}} \leq 2 \tag{20}$$

The reinforcement ratio is the geometric average of the reinforcement ratio in the y (ρ_{ly}) and x (ρ_{lx}) direction:

$$\rho_l = \sqrt{\rho_{lx} \cdot \rho_{ly}} \tag{21}$$

The lower bound of the shear capacity is a nationally determined parameter, with a recommended expression for v_{min} as

$$v_{min} = 0.035 k^{3/2} f_{ck}^{1/2} \tag{22}$$

The punching shear resistance of slabs with shear reinforcement is calculated as

$$v_{Rd,cs} = 0.75 v_{Rd,c} + 1.5 \left(\frac{d}{s_r} \right) A_{sw} f_{ywd,ef} \left(\frac{1}{U_1 d} \right) \sin \alpha \tag{23}$$

where A_{sw} is the area of one perimeter of shear reinforcement around the column; s_r is the radial spacing of perimeters of shear reinforcement; $f_{ywd,ef}$ is the effective design strength of the punching shear reinforcement; and α is the angle between shear reinforcement and the horizontal plane of the slab.

2.1.3. Model Code 2010

The *fib* Model Code 2010 punching shear provisions are based on the critical shear crack theory [15,16]. The design shear demand V_{Ed} acts on the basic control perimeter $b_{1,MC}$ at $0.5 d_v$ from the supported area, where d_v is the effective depth of the slab. Figure 7 illustrates the basic control perimeter for different supported areas.

(a)   **(b)**
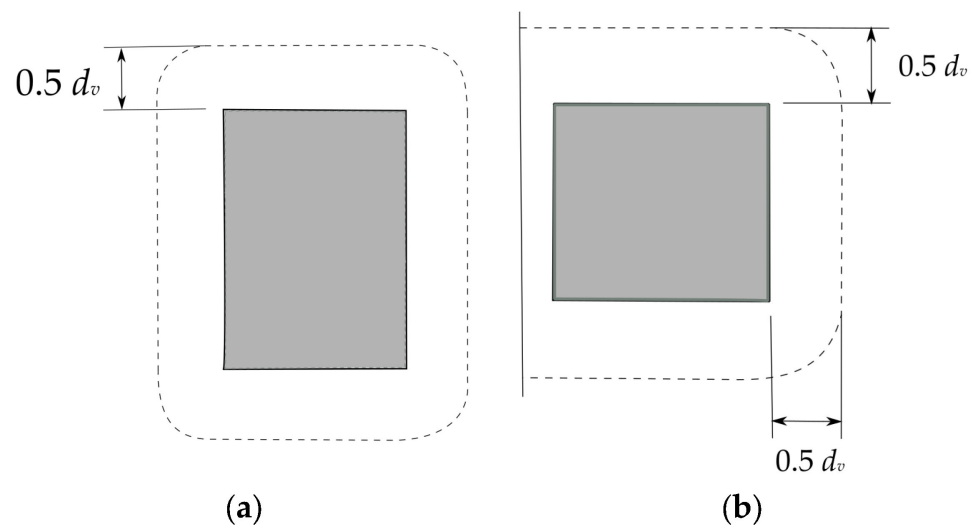
Figure 7. Basic control perimeter, modified from Ref. [9]: (**a**) interior column; (**b**) edge slab–column connection.

Then, for calculating the punching shear resistance of the slab, a control perimeter b_0 is used. This perimeter accounts for the non-uniform distribution of shear forces along $b_{1,MC}$, which can be caused by concentrations of the shear forces due to moment transfer between the slab and the supported area because of eccentricities in the load application [9]. Figure 8 illustrates the eccentricity of the resultants [9].
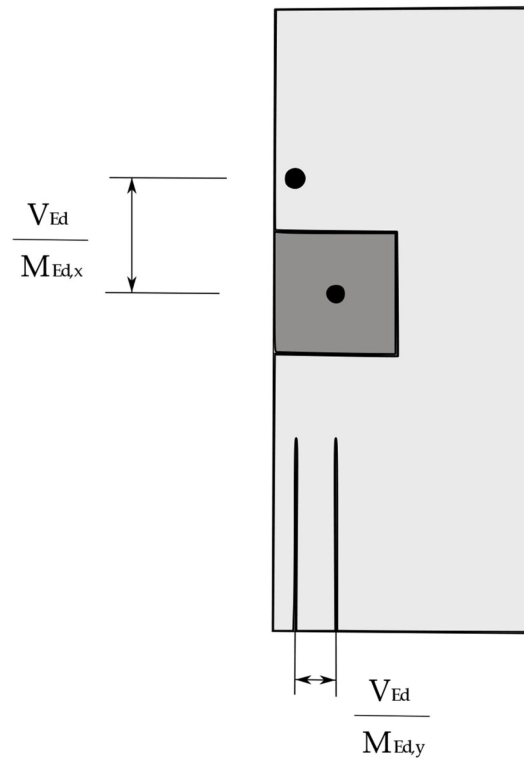
Figure 8. Resultant of shear forces, modified from Ref. [9].

The control perimeter b_0 is determined as

$$b_0 = k_e b_{1,MC} \tag{24}$$

The factor k_e represents the coefficient of eccentricity:

$$k_e = \frac{1}{1 + \frac{e_u}{b_u}} \tag{25}$$

where e_u is the eccentricity of the resultant shear forces with respect to the centroid of $b_{1,MC}$, and b_u is the diameter of a circle with the same area as the region inside $b_{1,MC}$.

The punching shear resistance V_{Rd} is calculated as

$$V_{Rd} = V_{Rd,c} + V_{Rd,s} \geq V_{Ed} \tag{26}$$

The design shear resistance attributed to the concrete is calculated using the following expression, with the compressive strength of the concrete, f_{ck}, in [MPa]:

$$V_{Rd,c} = k_\psi \frac{\sqrt{f_{ck}}}{\gamma_c} b_0 d_v \tag{27}$$

k_ψ is a parameter that depends on the rotations of the slab and shall be calculated as

$$k_\psi = \frac{1}{1.5 + 0.9 k_{dg} \psi d} \leq 0.6 \tag{28}$$

where d is the mean value of the effective depth of the slab for x and y directions, and k_{dg} shall be calculated as follows, with d_g in [mm]:

$$k_{dg} = \frac{32}{16 + d_g} \geq 1.15 \tag{29}$$

where d_g is the maximum aggregate size.

The design shear resistance attributed to the shear reinforcement is calculated as

$$V_{Rd,s} = \sum A_{sw} k_e \sigma_{swd} \sin \alpha \tag{30}$$

where $\sum A_{sw}$ is the sum of the area of all the shear reinforcement acting on the zone between $0.35d_v$ and d_v, which has a length of $0.65d_v$ (see Figure 9) [9].
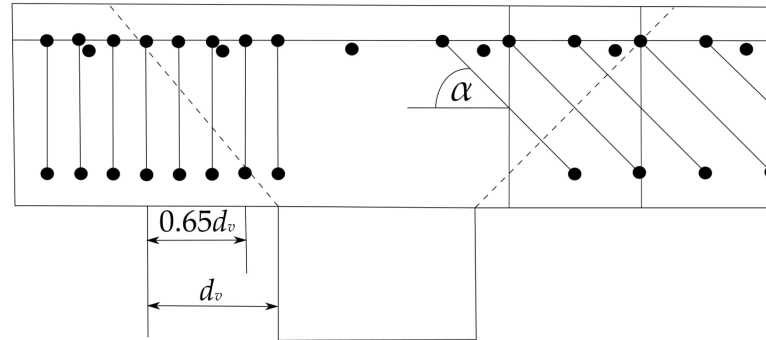
Figure 9. Shear reinforcement resisting shear crack, based on Ref. [9].

The stress σ_{swd} is calculated as

$$\sigma_{swd} = \frac{E_s \psi}{6} \le f_{ywd} \tag{31}$$

where f_{ywd} is the yield strength.

The load-rotation behavior of the slab is calculated as follows:

$$\psi = 1.5 \frac{r_s}{d} \frac{f_{yd}}{E_s} \left(\frac{m_{sd}}{m_{Rd}} \right)^{1.5} \tag{32}$$

where r_s is the distance from the column axis to the line of contra-flexure of the radial bending moments; f_{yd} is the yield strength of the flexural reinforcement; E_s is the modulus of elasticity of the flexural steel; m_{sd} is the average moment per unit length for calculating flexural reinforcement in the support strip; and m_{Rd} is the average flexural strength per unit length in the support strip [9]. The values of the mechanical parameters in the formula can be calculated with different levels of approximation (LoA), where increasing levels of approximation indicate increasing precision but also increasing computational time and effort [6].

LoA I assumes that $m_{sd} = m_{Rd}$, which implies that the strength of the slab will be governed by its bending moment capacity. For regular slabs with a long-to-short span length ratio $0.5 \le L_x/L_y \le 2.0$, r_s can be estimated as follows:

$$r_{sx} = 0.22L_x; \; r_{sy} = 0.22L_y \tag{33}$$

Figure 10 illustrates L_x and L_y [9].

LoA II includes a simplified estimation of m_{sd}. LoA III replaces the coefficient 1.5 in Equation (32) with 1.2 if r_s and m_{sd} are calculated with a linear elastic model. LoA IV is based on a nonlinear analysis of the structure, and it considers cracking, tension-stiffening effects, yielding of the reinforcement and any other relevant nonlinear effects [9]. LoA III was used for the present investigation.
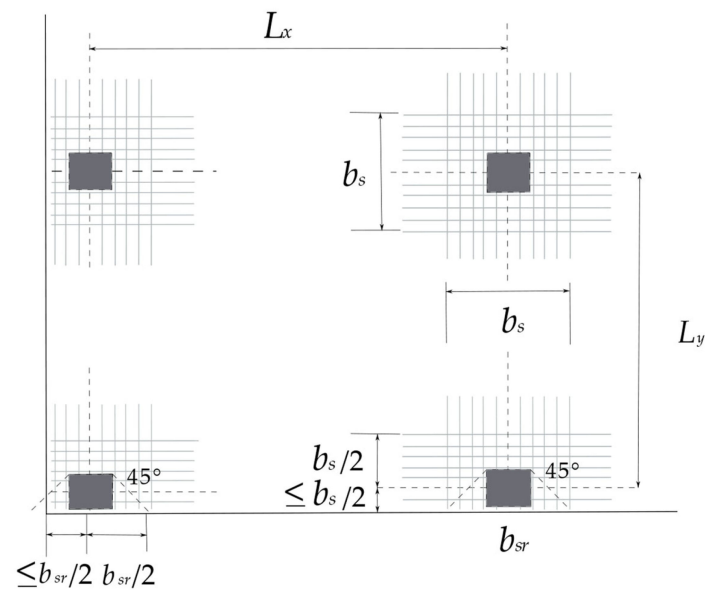
Figure 10. Slab dimensions and support strip dimensions, modified from Ref. [9].

2.2. Database of Eccentric Punching Shear Experiments

2.2.1. Development of the Database

The database developed for this study contains 128 experiments of eccentric punching shear on flat slabs with longitudinal reinforcement and with or without transverse shear reinforcement reported in the literature. The references consulted are works by Krüger [2], Moe [11], Albuquerque et al. [17], Hammill and Ghali [18], Narayani [19], Zaghlool [20], Anis [21], Hanson and Hanson [22], Stamenkovic [23], Pina Ferreira [24], Ritchie [25], Sudarsana [26], Zaghloul [27], Desayi [28], Walker [29] and Stamenkovic [30]. Tables A1–A7 present the database developed for this study, see Appendix A. The full spreadsheet is available in the public domain in .xlsx format [31]. The notations used in this database are given in the "List of notations". Figure 11 illustrates the different slab geometries and slab–column connections found in the literature [2,11,17–30].

(a)
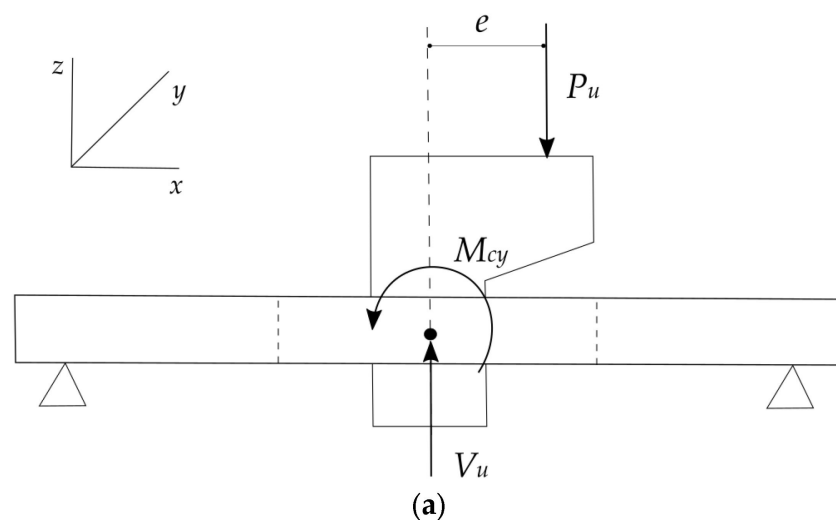
Figure 11. *Cont.*
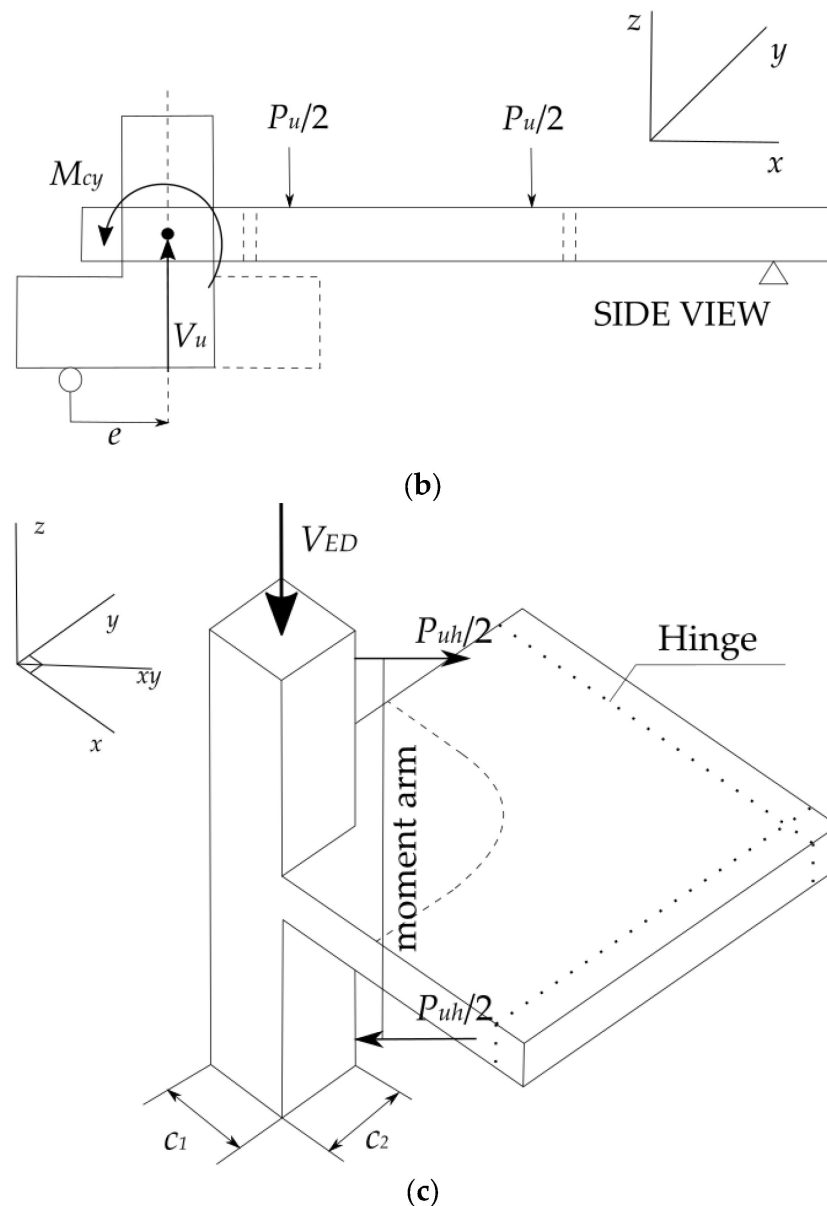
Figure 11. Slab geometries and test slab–column connection: (**a**) square interior slab–column connection [19]; (**b**) rectangular edge slab–column connection [17]; (**c**) square corner slab–column connection [18].

For Refs. [2,17,18,22,24,25,28,29], the age of the specimens at the time of testing was not provided, and thus, it is assumed to be 28 days. For Refs. [2,11,18,21–23,25–30], the tensile strength of the concrete f_{ct} was not reported by the authors. To complete this information, the expression developed by Sarveghadi [32] was used:

$$f_{ct} = 0.76\sqrt{f_c} \tag{34}$$

with f_c as the cylinder concrete compressive strength in [MPa].

For Refs. [18,19,23,25,28–30], the modulus of elasticity of the flexural reinforcement was not provided; for Refs. [18,23,25,28–30], it was assumed as 200 GPa, and for Ref. [19], it was estimated from the stress–strain graph reported by the author.

Refs. [2,17–19,24,27] present slabs with transverse shear reinforcement; stirrups, shear hats (see Figure 12) and studs were the shear reinforcement types found in these works.
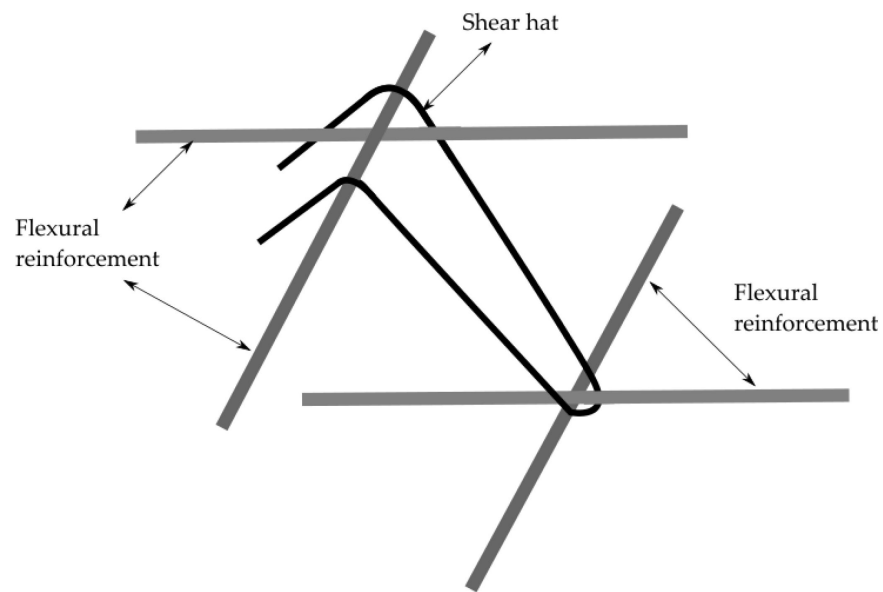
Figure 12. Shear hat setup, as used in Ref. [19].

For internal slab–column connections, Refs. [2,11,19] presented the ultimate load applied to the slab–column connection and its eccentricity; on the other hand, Refs. [21–24] reported the ultimate moment applied to the slab–column connection. For the edge slab–column connections, Refs. [17,19,22] presented the ultimate load applied to the slab–column connection and its eccentricity, and Refs. [20,23,25–27] reported the ultimate moment applied to the slab–column connection. Finally, for corner slab–column connections, Refs. [18,20,26,30] reported the ultimate moment applied to the slab–column connection. In all the works, the test setup caused this moment to act diagonally on the slab. Figure 11c illustrates this type of loading. On the other hand, Refs. [28,29] reported the ultimate load applied to the slab–column connection and its eccentricity. For the database, the diagonally applied moment was divided into its components in the x and y directions. All values in the database are presented in SI units. The information from Refs. [11,20–23,30] was converted from US customary to SI units.

2.2.2. FEM Modeling Process

The FEM models were developed in Scia Engineer [33] as similar to the reported experiments as possible, including the contribution of the self-weight when testing occurred in the gravity direction (i.e., self-weight increases sectional shear).

To model the slab–column connections, rigid line links were placed through the center of the column on the y and x axis. The result of a rigid link is that the deformation of both nodes in the direction of the line connecting both nodes will be identical, and the orientation of the line connecting both nodes after the calculation depends on the selected type of rigid link [33]. The average size for two dimensional elements on the models was 0.01 m.

For test setups where the load was applied directly to the slab, free node point loads were applied on the model. On the other hand, when loads were applied to the column in the experiments, point loads were applied similarly in the FEM models; this applies to vertical and horizontal loads. The results presented in Tables A8–A10 are the maximum shear internal forces of the slab at failure, measured on the punching perimeter described in the ACI 318-19 code [7] divided by the effective depth of the slab d. Figure 13 illustrates the various steps in the process.

(**a**)

(**b**)

(**c**)

Figure 13. *Cont.*

(**d**)
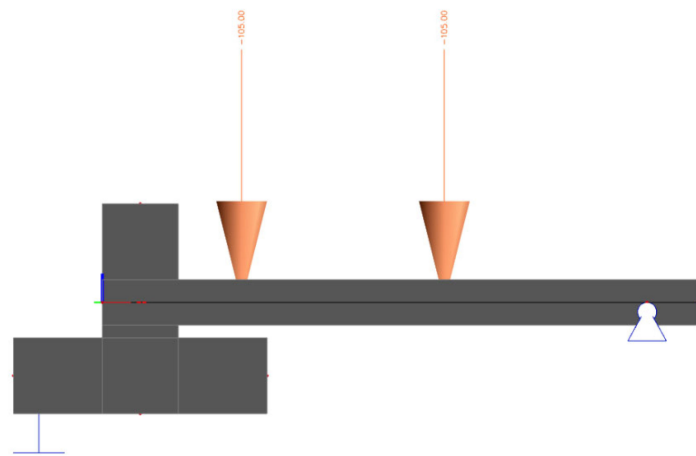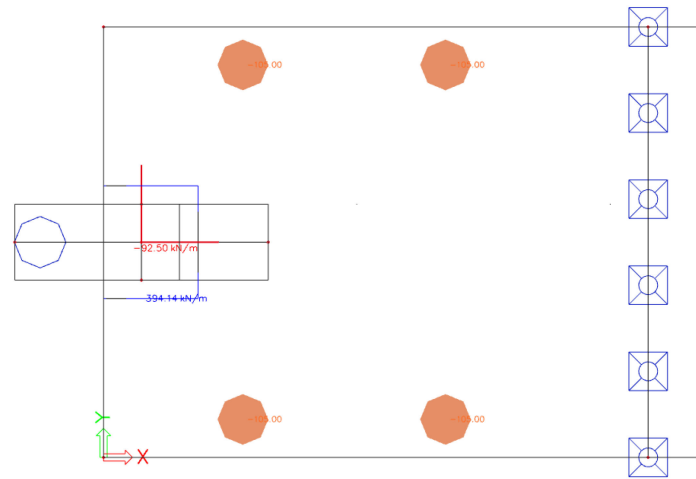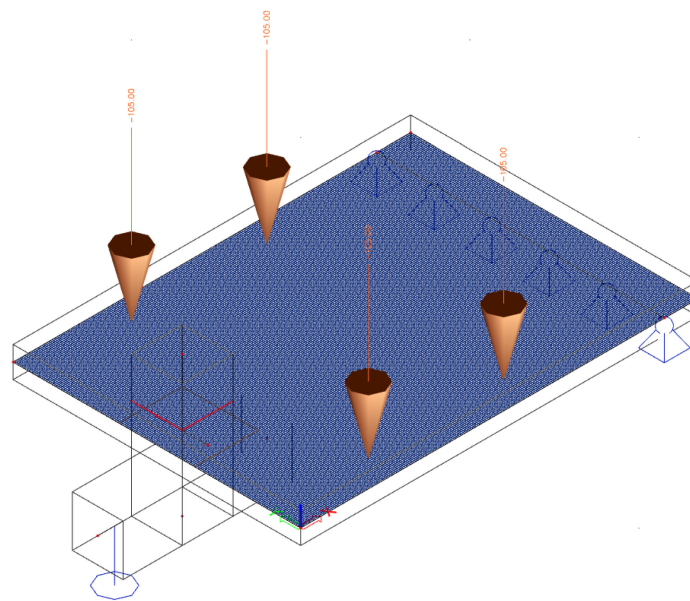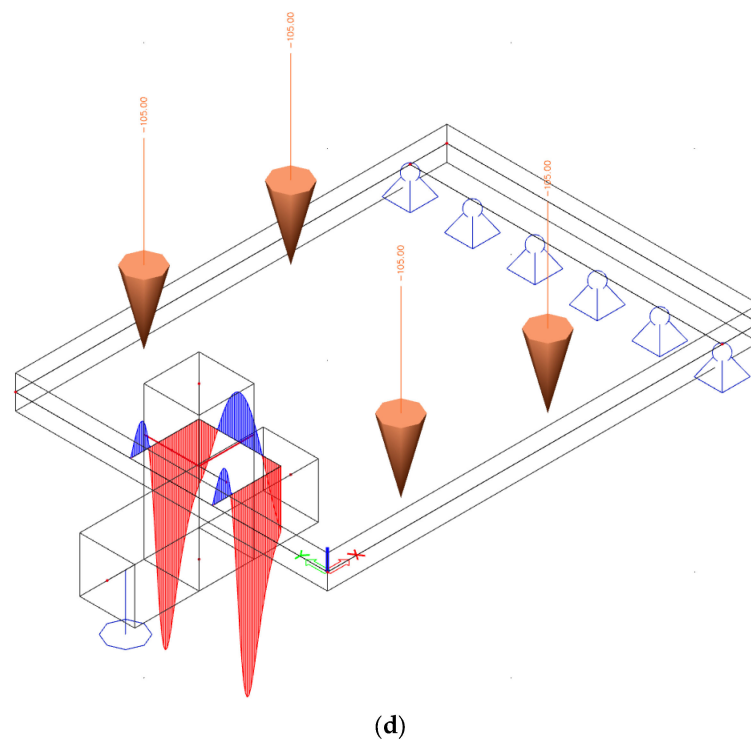
Figure 13. Example of finite element analysis on an Albuquerque [17] specimen: (**a**) Applied loads in the model and support conditions (side view); (**b**) Rigid line links on the column *x* and *y* axis, punching perimeter defined by ACI 318-19 code [7] (plan view); (**c**) Mesh generation (diagonal view); (**d**) Internal shear stress on the critical perimeter, calculated from the applied load and the self-weight of the specimen.

The internal, edge and corner specimens followed the same modeling process. Figure 14 shows the typical shear stress distributions around the control perimeter considered; note that the loads applied are displayed to show the loading eccentricity.

(**a**)

Figure 14. *Cont.*

(**b**)

(**c**)
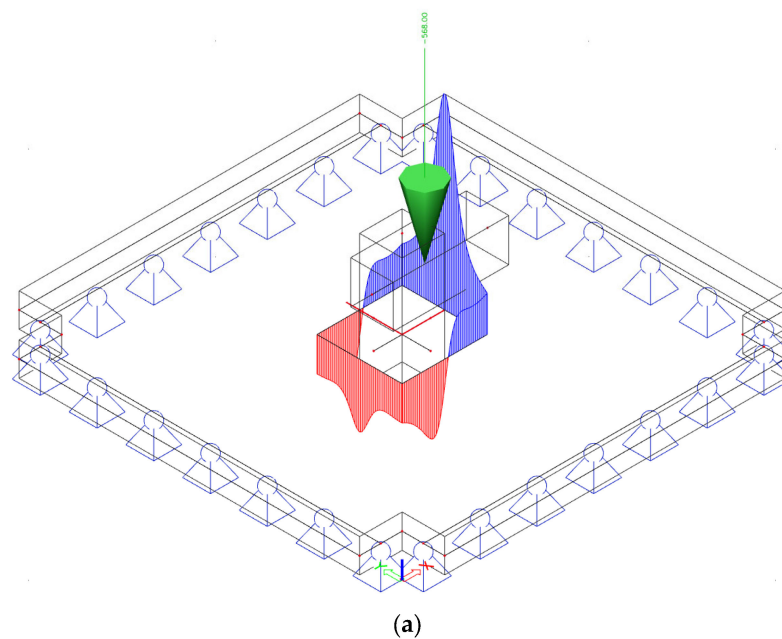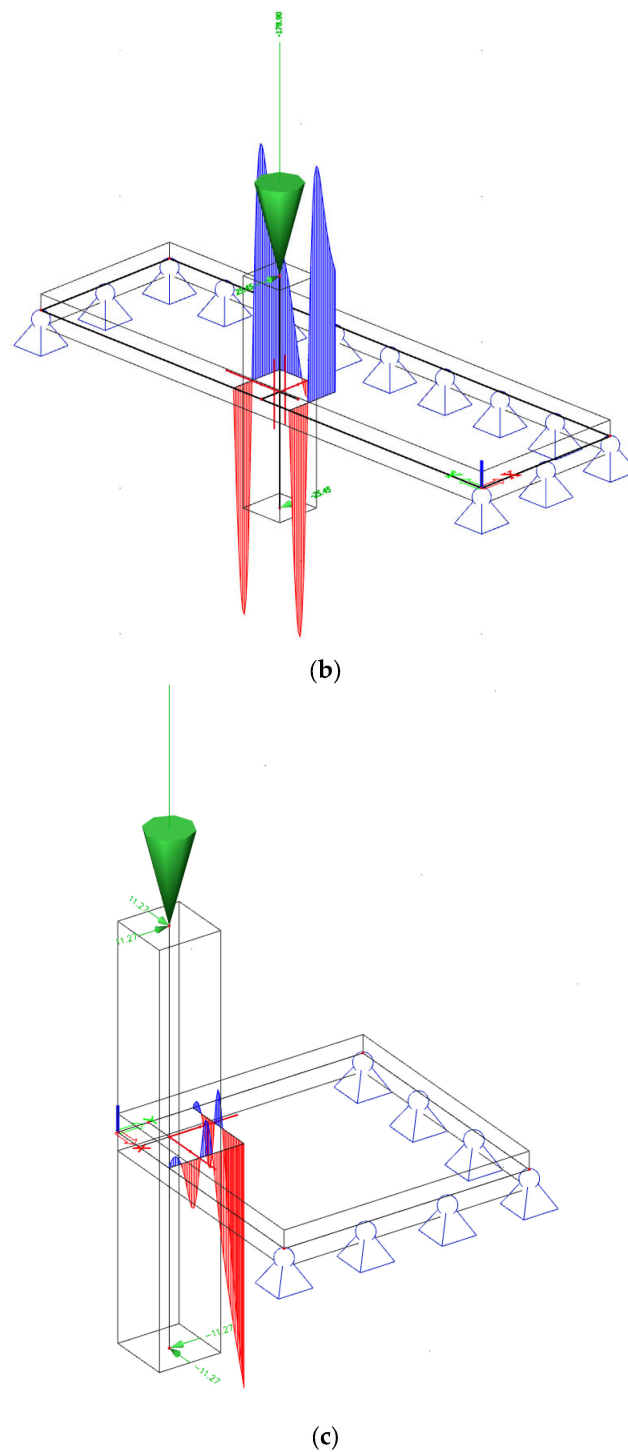
Figure 14. Example of typical shear stress distributions around the control perimeter defined by ACI 318-19 code [7]: (**a**) Internal slab–column connection; (**b**) Edge slab–column connection; (**c**) Corner slab–column connection.

2.2.3. Parameter Ranges in the Database

In this section, an evaluation of the distribution of the values of the parameters in the database is made. Table 1 gives the ranges of the most important parameters in the database. The value of ρ_l is either taken directly from the referenced work, where available, or calculated as the geometric average of the longitudinal and transverse reinforcement ratios.

Table 1. Ranges of parameters in the database.

Parameter	Min	Max	Mean	Median	STD
L_x (mm)	530	3000	1275	1075	631
L_y (mm)	530	3000	1383	1525	632
h (mm)	76	180	126	150	39
d (mm)	56	151	98	114	33
ρ_l (%)	0.53%	2.23%	1.3%	1.2%	0.3%
f_c (MPa)	15.5	59.3	37.4	37.0	8.8
d_g (mm)	9.5	38.1	13.2	10.0	7.8
a (mm)	419	2000	905	860	422
a_v (mm)	343	1850	788	749	405

Figure 15 shows the distribution of the most important parameters in the database. Figure 15a shows that the majority of the slabs are made of normal strength concrete. The developed database cannot be used to gain insight into the eccentric punching shear capacity of high-strength concrete slab–column connections. Figure 15b shows that a tensile reinforcement ratio in the range of 1.25–1.50% was commonly used in the tested slabs. Typical slab designs use reinforcement ratios of 0.6–0.8%. None of the experiments in the database used these practical values, with most slabs being over-reinforced in flexure to achieve a punching shear failure. The distribution of the average effective depth of the slabs is presented in Figure 15c. This plot shows that at least half of the specimens had an effective depth d in the range 100 mm–125 mm, and another large portion of the specimens had an effective depth close to 75 mm. The reported specimens are small-scale specimens that do not give us insights regarding the size effect for eccentric punching shear. Figure 15d shows the ratio between the shear span and the average effective depth a/d. The range of a/d in the experiments covers only situations in which no direct load transfer can occur; as such, for this database, there is a consistency in the range of a/d. Figure 15e shows the maximum aggregate size values reported in the literature. The values reported are consistent with the values shown in Figure 15c; relatively small maximum aggregate sizes are used for the fabrication of specimens with small depths.

(a)

(b)

Figure 15. *Cont.*

(c)

(d)

(e)
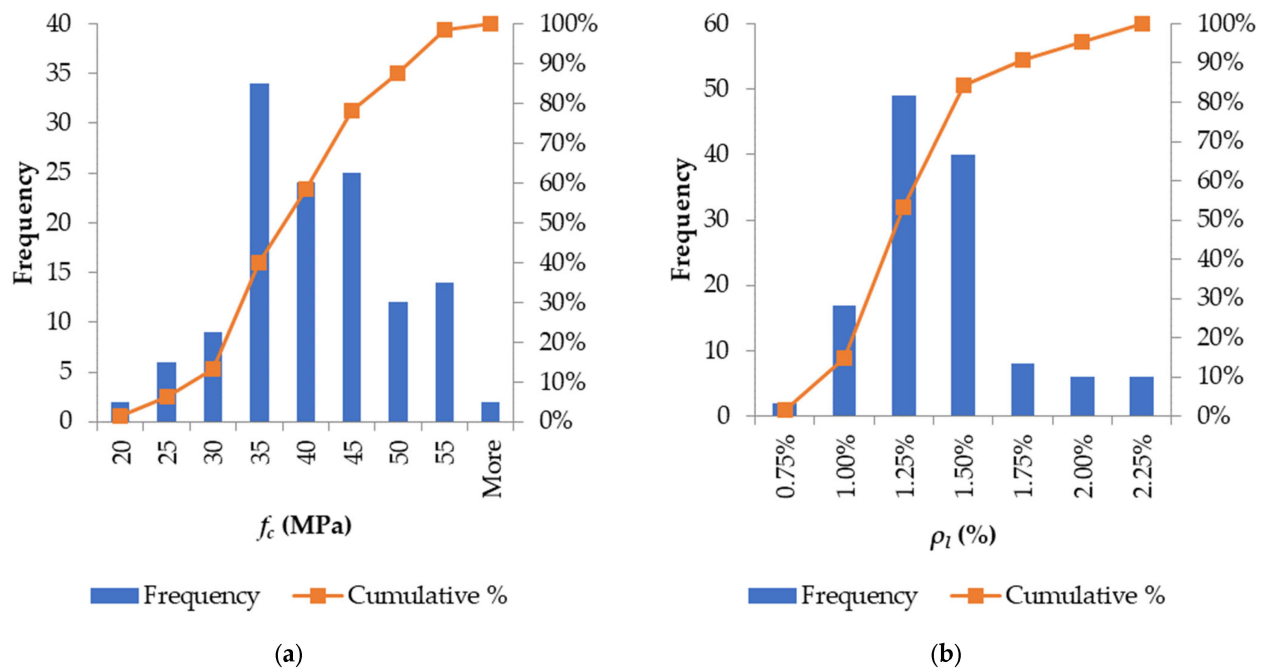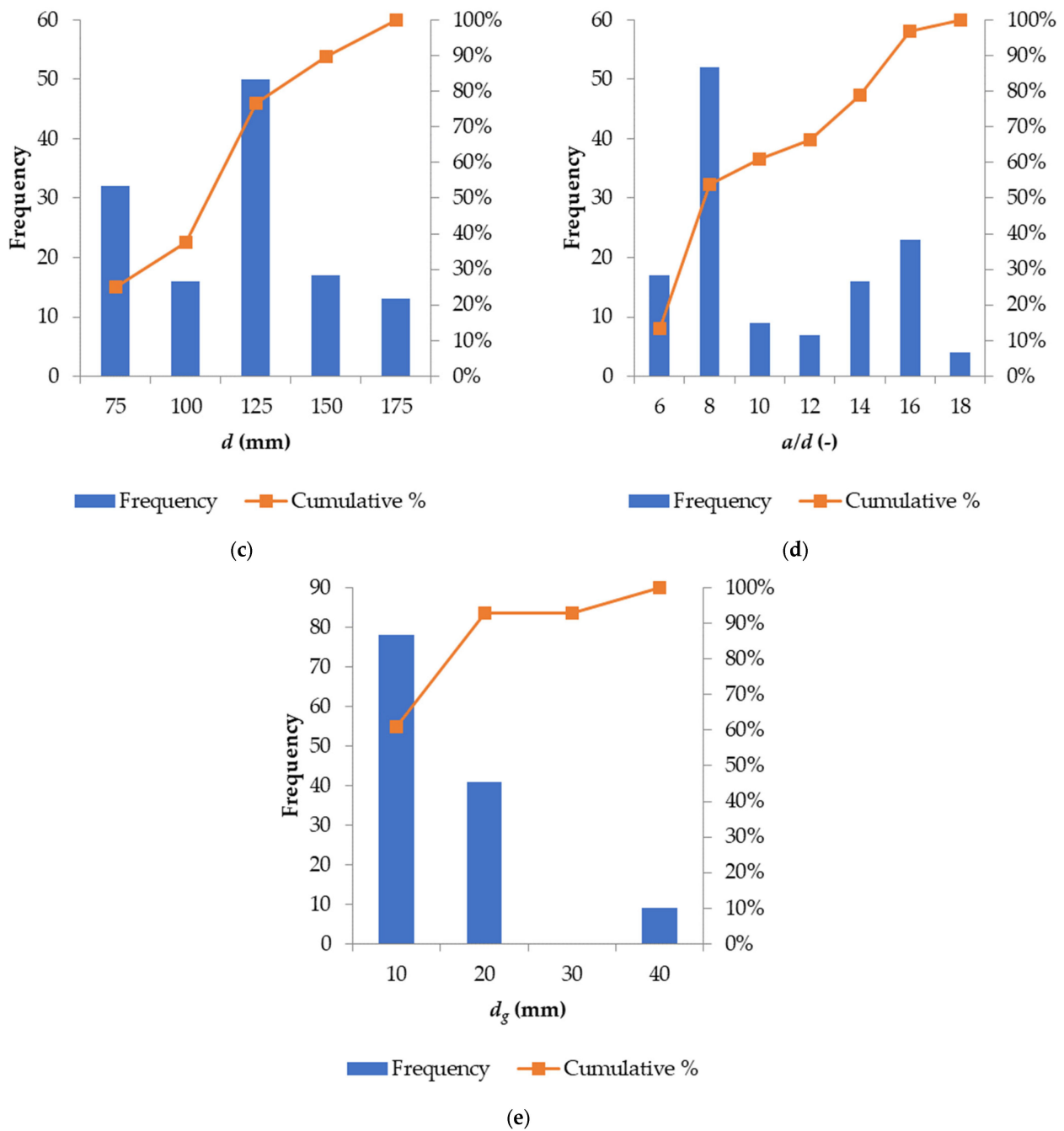
Figure 15. Distribution of the most important parameters in the database: (**a**) concrete compressive strength f_c; (**b**) tensile reinforcement ratio ρ_l; (**c**) effective depth d; (**d**) shear span to average effective depth ratio a/d; (**e**) maximum aggregate size d_g.

3. Results

3.1. Parameters Studied

The raw data from the database are used to analyze the effect of different experimental parameters on the sectional shear stress at failure. The ACI 318-19 [7] expression (Equation (1)) is used for determining the shear stress on the perimeter v_u. Normalized shear stresses are used to discard the influence of the concrete compressive strength f_c. An analysis of the shear stress normalized to the square root and to the cubic root of the concrete compressive strength is carried out first. Figure 16a,b show the relation between the normalized shear strength and f_c, and, as can be seen, for the experimental results

studied, normalizing the shear strength to the square root of the concrete compressive strength is preferable. A similar observation was made for the shear capacity of steel fiber reinforced concrete beams [34].

(**a**)

(**b**)
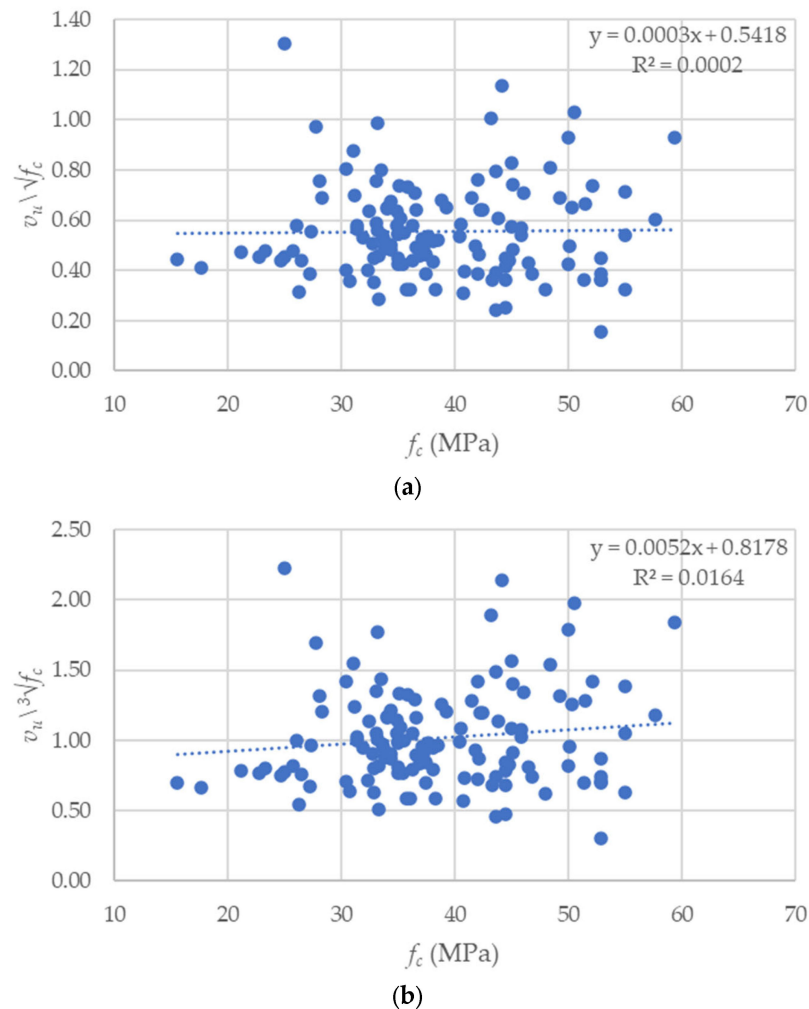
Figure 16. Shear stresses normalized to the concrete compressive strength: (**a**) normalized to the square root; (**b**) normalized to the cubic root.

Thus, the influence of different important parameters is studied as a function of the shear stress normalized to the square root of f_c. Figure 17 shows the influence of the most important parameters on the shear stress normalized to the square root of f_c. Figure 17a shows the influence of the effective depth d on the normalized shear stress. For the specimens in the database compiled, the influence of the effective depth on the normalized shear capacity is negligible. However, experiments on slabs with a larger effective depth are not available; therefore, this database cannot give insights regarding the size effect in eccentric punching shear. Figure 17b shows the influence of the reinforcement ratio ρ_l. Larger reinforcement ratios result in larger shear capacities, as expected. As more tension reinforcement is provided, the contribution of dowel action to the shear capacity increases. Other factors that could explain the influence of the reinforcement ratio on the shear capacity are improved aggregate interlock due to a reduction in crack width for specimens with more flexural reinforcement, and a larger contribution of the uncracked concrete zone due to an increase in the flexural compression block depth. However, the overall scatter on the trendline is large. Figure 17c shows the influence of the shear span to the effective depth a/d. For the experiments in the database compiled, this parameter had negligible influence on the normalized shear stress.

(a)

(b)

(c)
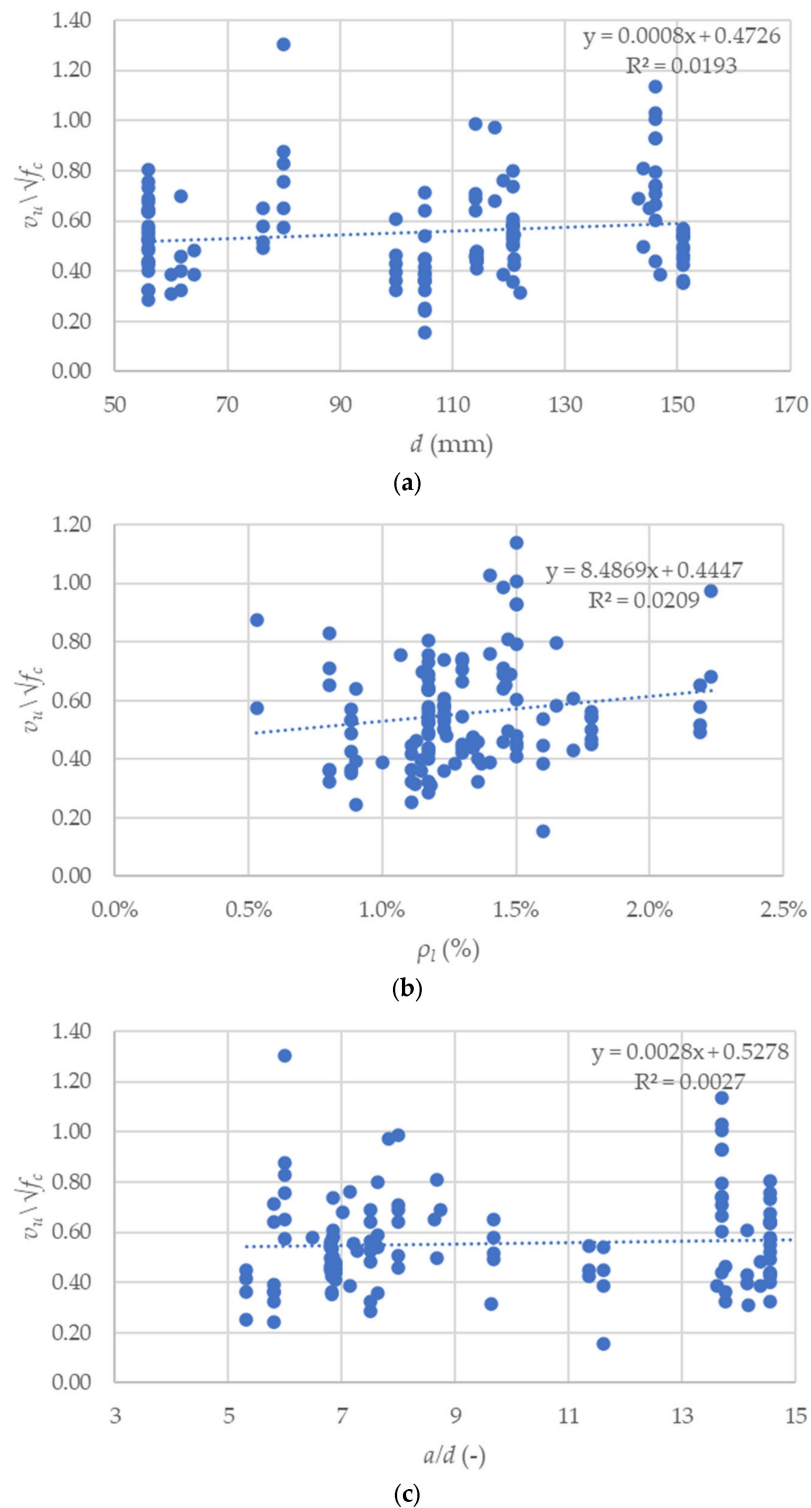
Figure 17. Parameter studies based on the normalized shear stress at failure of all entries in the database: (**a**) effective depth *d*; (**b**) longitudinal reinforcement ratio ρ_l; (**c**) shear span to depth ratio *a/d*.

3.2. Comparison with Code Predictions

The measured shear capacities from the database are then compared with the shear capacities predicted by three different codes: ACI 318-19 [7], NEN-EN 1992-1-1:2005 [8] and the *fib* Model Code 2010 [9]. Figure 18 shows the comparison between the tested and predicted results, with the statistical properties of the tested-to-predicted shear stresses

in Tables 2–4. Figure 19 shows the comparison between the SCIA Engineer [33] FEM results v_{FEM} and the predicted shear capacities v_{pred} for ACI 318-19 [7], with the statistical properties of this comparison in Table 5. The FEM results of the shear stress were compared only to ACI 318-19 [7], as NEN-EN 1992-1-1:2005 [8] and *fib* Model Code 2010 [9] assume a plastic stress distribution on the punching perimeter. ACI 318-19 [7], on the other hand, assumes a linear stress distribution. The results of the linear finite element analysis were compared to check the alignment of the assumptions of linear behavior. The results for all the entries of the database are presented in Tables A8–A10. Some experiments only use the moment on the slab-column connection and do not use a load on the slab. For these referenced works, the NEN-EN 1992-1-1:2005 [8] and fib Model Code 2010 [9] models were not evaluated. Equation (14) from NEN-EN 1992-1-1:2005 [8] uses the value of shear force applied to the slab–column connection for calculating the enhancement factor for eccentric shear, β_{EC}, so that the shear stress caused by unbalanced moment only cannot be determined. The same problem arises when applying Equations (24) and (25) from the *fib* Model Code 2010 [9]; the eccentricity e_u is calculated from the resultant shear forces applied to the slab–column connection.
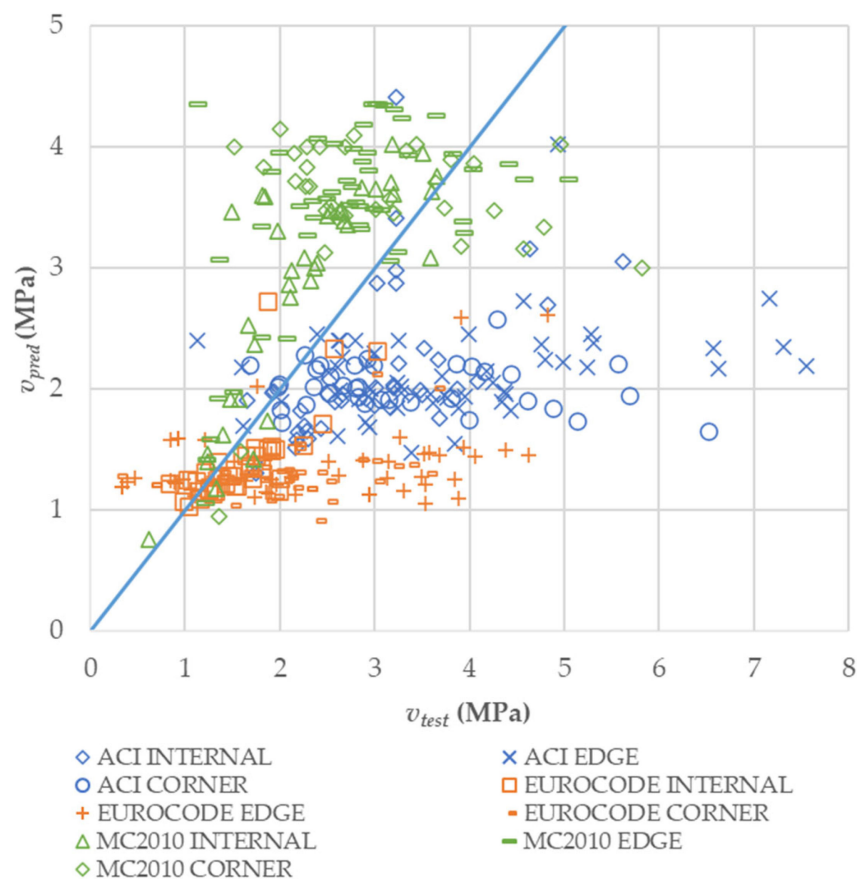
Figure 18. Comparison between experimental v_{test} and predicted shear capacities v_{pred} for three design methods from existing codes.

The validation of the spreadsheet used for calculating the code predictions is available in the public domain [35].

In Table 2, the statistical results are first presented in general and are then presented separately by the type of slab–column connection being analyzed. The number of experiments evaluated varies from code to code because specimens that were not tested under direct shear could not be evaluated by NEN-EN 1992-1-1:2005 [8] and Model Code 2010 [9].

Table 2. Statistical results from the comparison between the tested and predicted capacities, Part I. The number of specimens used for the evaluation is shown within brackets. First, all results are shown together. Then, the results are subdivided into interior slab–column connections with unbalanced moment, edge slab–column connections and corner slab–column connections.

	AVG	STD	COV (%)
All Results			
ACI (128)	1.65	0.58	35.39
EC2 (122)	1.52	0.69	45.38
MC2010 (122)	0.82	0.24	29.63
Internal slab–column connections			
ACI (37)	1.41	0.31	22.27
EC2 (37)	1.15	0.22	19.00
MC2010 (37)	0.81	0.17	20.47
Edge slab–column connections			
ACI (55)	1.79	0.61	33.78
EC2 (51)	1.70	0.88	51.93
MC2010 (51)	0.79	0.21	26.20
Corner slab–column connections			
ACI (36)	1.67	0.69	41.18
EC2 (34)	1.66	0.54	32.75
MC2010 (34)	0.88	0.34	38.70

Table 3. Statistical results from the comparison between the tested and predicted capacities, Part II. The number of specimens used for the evaluation is shown within brackets. First, all results are shown together. Then, the results are subdivided into interior slab–column connections with unbalanced moment, edge slab–column connections and corner slab–column connections.

	AVG	STD	COV (%)
Slabs without Shear Reinforcement			
ACI (110)	1.65	0.58	35.24
EC2 (104)	1.51	0.68	45.17
MC2010 (104)	0.80	0.25	30.70
Internal slab–column connections			
ACI (28)	1.45	0.28	19.43
EC2 (28)	1.15	0.23	19.71
MC2010 (28)	0.77	0.15	19.25
Edge slab–column connections			
ACI (48)	1.78	0.62	34.60
EC2 (44)	1.64	0.86	52.58
MC2010 (44)	0.79	0.22	27.57
Corner slab–column connections			
ACI (34)	1.63	0.67	41.16
EC2 (32)	1.66	0.56	33.56
MC2010 (32)	0.86	0.34	39.07

Table 4. Statistical results from the comparison between the tested and predicted capacities, Part III. The number of specimens used for the evaluation is shown within brackets. First, all results are shown together. Then, the results are subdivided into interior slab–column connections with unbalanced moment, edge slab–column connections and corner slab–column connections.

	AVG	STD	COV (%)
Shear-Reinforced Slabs			
	AVG	STD	COV (%)
ACI (18)	1.64	0.61	37.32
EC2 (18)	1.59	0.75	47.54
MC2010 (18)	0.93	0.20	21.35
Internal slab–column connections			
	AVG	STD	COV (%)
ACI (9)	1.30	0.40	30.64
EC2 (9)	1.18	0.21	17.65
MC2010 (9)	0.93	0.16	17.14
Edge slab–column connections			
	1.89	0.57	30.02
ACI (7)	2.10	0.99	46.99
EC2 (7)	0.83	0.14	17.27
MC2010 (7)	1.89	0.57	30.02
Corner slab–column connections			
	AVG	STD	COV (%)
ACI (2)	2.29	0.90	39.09
EC2 (2)	1.61	0.29	18.30
MC2010 (2)	1.25	0.26	20.88

◇ ACI Tested/Predicted INTERNAL   □ ACI Tested/Predicted EDGE
△ ACI Tested/Predicted CORNER   × FEM/ACI Predicted INTERNAL
○ FEM/ACI Predicted EDGE   ○ FEM/ACI Predicted CORNER
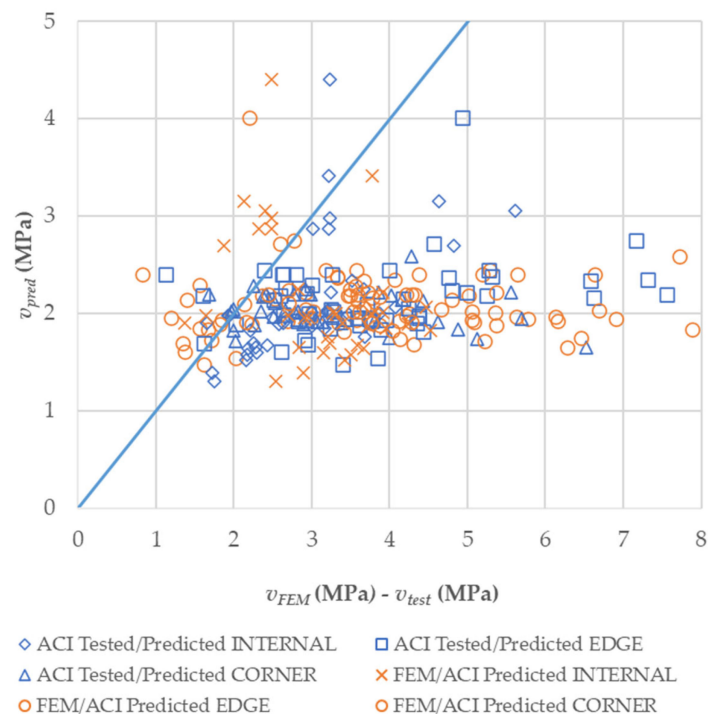
Figure 19. Comparison between the SCIA Engineer [33] FEM results and the predicted shear capacities for ACI 318-19 [7].

Table 5. Statistical results from the comparison between SCIA Engineer [33] FEM results for the acting shear stress and the predicted shear capacities for ACI 318-19 [7].

	AVG	STD	COV (%)
All specimens	1.81	0.85	46.94
Internal slab–column connections	1.70	0.85	50.02
Edge slab–column connections	1.57	0.66	42.15
Corner slab–column connections	2.30	0.93	40.18

In Table 3, the statistical results are first presented in general and are then presented separately by the type of slab–column connection being analyzed. The number of experiments evaluated varies from code to code because specimens that were not tested under direct shear could not be evaluated by NEN-EN 1992-1-1:2005 [8] and Model Code 2010 [9].

In Table 4, the statistical results are first presented in general and are then presented separately by the type of slab–column connection being analyzed. The number of experiments evaluated varies from code to code because specimens that were not tested under direct shear could not be evaluated by NEN-EN 1992-1-1:2005 [8] and Model Code 2010 [9].

As can be observed in Table 2, ACI 318-19 [7] and NEN-EN 1992-1-1:2005 [8] tend to be on the conservative side in terms of the average tested to predicted shear stresses. The Model Code 2010 [9] predicted shear capacities that are on average below the tested shear stress at failure (average = 0.82). Considering the overall results, the Model Code 2010 [9] also has the smallest coefficient of variation (COV = 29.63%) on the tested to predicted shear stresses. These results could be considered generally unsatisfactory. Nevertheless, all three codes performed better when evaluating only internal slab–column connections without shear reinforcement, with COV values under 20% for all. The tested to predicted values using NEN-EN 1992-1-1:2005 [8] show the lowest maximum value for one entry (0.24); however, the tested to predicted value using the Model Code 2010 [9] for this entry is small as well (0.58). The entry analyzed is named C/C/4, from Ref. [30], and it is a corner slab–column connection, unreinforced in shear (see Table A8 in Appendix B).

All three models evaluated performed differently when predicting strengths on internal, edge and corner slab–column connections. ACI 318-19 [7] and NEN-EN 1992-1-1:2005 [8] tend to render more conservative results for edge and corner slab–column connections, as shown in Tables 3 and 4. NEN-EN 1992-1-1:2005 [8] showed the largest scatter when evaluating edge slab–column connections (COV = 51.93%), which is considered unacceptable.

As can be observed in Figure 19 and Table 5, the ACI 318-19 [7] assumption of a linear elastic model distribution leads to an overestimation of the real performance of the specimens. Replacing the shear stresses calculated assuming a linear stress distribution with the results presented in Tables A8–A10, which are the maximum shear internal forces of the slab at failure, measured on the punching perimeter described in the ACI 318-19 code [7] divided by the effective depth of the slab *d* in the comparison to the shear capacity from ACI 318-19 (see Table 5), results in larger (i.e., more overly conservative) values for the tested to predicted shear. At the same time, the COV on the tested to predicted values increases, indicating that when using ACI 318-19, both the shear stress from the code provisions and the shear capacity should be used together. Using the results from the FEM models, increasing the level of precision of the assumption of a linear elastic model distribution, which was demonstrated to lead to an overestimation of the shear capacity of the slab, tends to enlarge this overestimation.

As can be observed in Figure 20 and Table 6, the ACI 318-19 [7] assumption of a linear elastic model distribution does not hold up for finer calculations using the SCIA Engineer [33] FEM results. Although the average value for the comparison between the shear capacities for ACI 318-19 [7] and SCIA Engineer [33] FEM results for the acting shear stress is relatively close to 1.0, the COV on these results is not acceptable (COV = 54.37) (see Tables A11–A13).
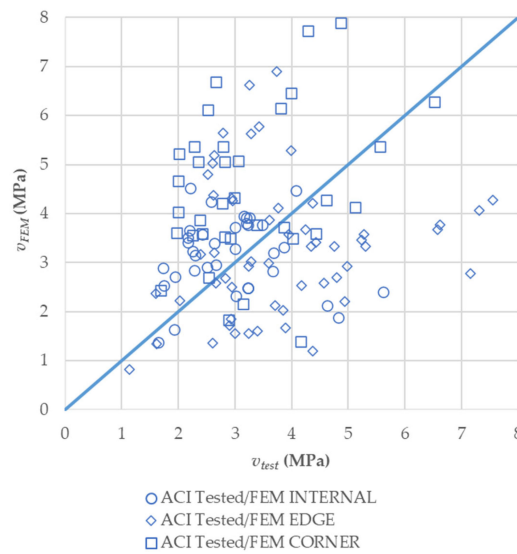
Figure 20. Comparison between the SCIA Engineer [33] FEM results and the shear stress for ACI 318-19 [7], calculated using Equation (1).

Table 6. Statistical results from the average value for the comparison between the acting shear stress for ACI 318-19 [7] and SCIA Engineer [33] FEM results for the acting shear stress.

	AVG	STD	COV (%)
All specimens	1.09	0.59	54.37
Internal slab–column connections	0.99	0.49	49.09
Edge slab–column connections	1.33	0.63	47.85
Corner slab–column connections	0.82	0.48	58.59

3.3. Influence of Parameters on Tested to Predicted Punching Capacities

Figure 21 shows the v_{test}/v_{pred} values as a function of the different parameters, studied in Section 3.1, for the various codes with the objective of obtaining an insight in which codes over- or underestimate the various parameters.

(a)

Figure 21. *Cont.*

(b)

(c)

Figure 21. *Cont.*

(d)

(e)
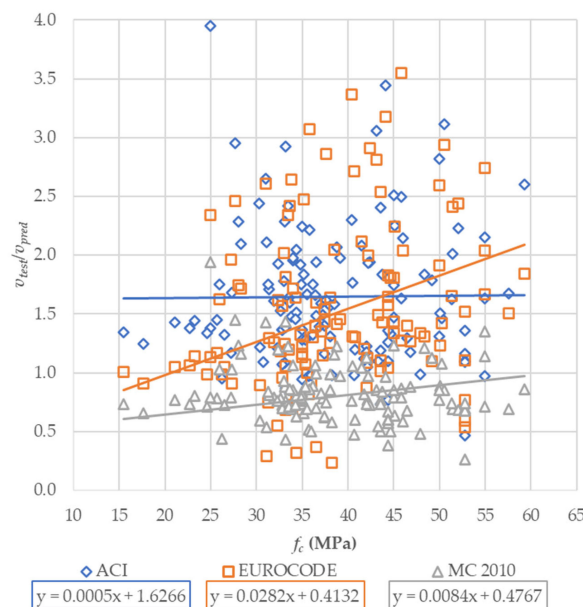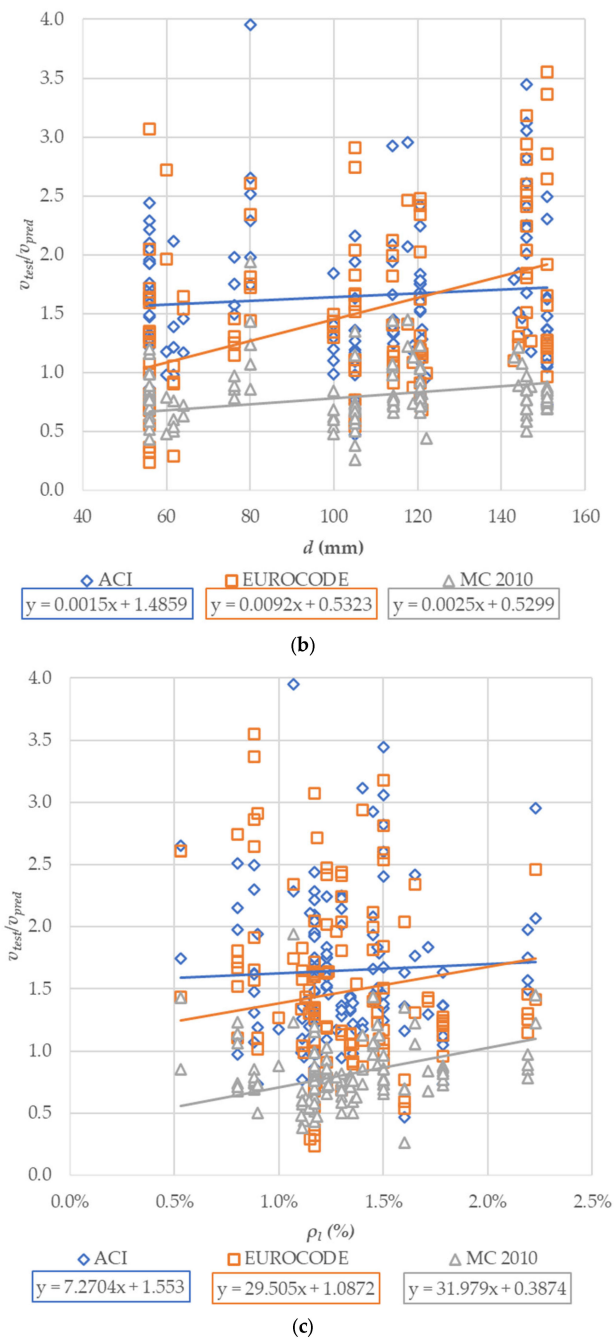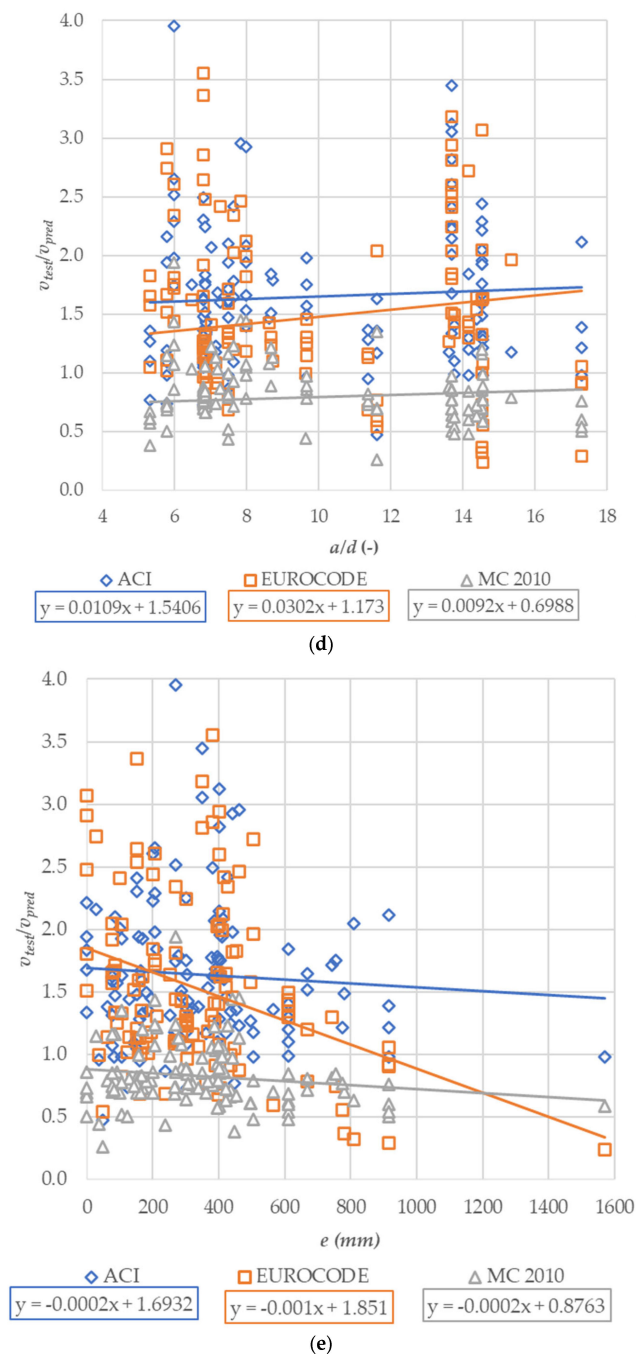
Figure 21. Parameters studied based on the comparison between experimental v_{test} and predicted shear capacities v_{pred} for three design methods from existing codes: (**a**) concrete compressive strength f_c; (**b**) effective depth d; (**c**) longitudinal reinforcement ratio ρ_l; (**d**) shear span to depth ratio a/d; (**e**) eccentricity.

As can be observed in Figure 21a, ACI 318-19 [7] tends to underestimate the influence of the compressive strength of the concrete f_c. On the other hand, the *fib* Model Code [9] and NEN-EN 1992-1-1:2005 [8] correctly take the influence of the concrete compressive strength into account.

When considering the influence of the effective depth d on the tested to predicted ratios (Figure 21b), we can see that NEN-EN 1992-1-1:2005 [8] and the *fib* Model Code [9] take the size effect correctly into account for the specimens tested. In contrast, for ACI 318-19 [7], no influence of size is considered. Additionally, we observe an important increase in the

conservativism of NEN-EN 1992-1-1:2005 [8] as the effective depth increases. For the tested sizes, the value of d only influences the size and location of the punching perimeter. None of the specimens were of a thickness at which the size effect factor from the code equations starts to play a role.

As can be seen in Figure 21c, NEN-EN 1992-1-1:2005 [8] and the *fib* Model Code 2010 [9] consider that the influence of the longitudinal reinforcement is larger than that observed in the experiments. The influence is taken into account more realistically in ACI 318-19 [7]. As the specimens in the database contained large reinforcement ratios, experiments on slabs with lower reinforcement ratios are necessary to further study the effect of the reinforcement ratio on the tested to predicted ratios determined with the studied codes.

Figure 21d shows that, for the Model Code 2010 [9] and NEN-EN 1992-1-1:2005 [8], as the shear span to depth ratio a/d increases, the values of v_{test}/v_{pred} tend to become more conservative. On the other hand, for ACI 318-19 [7], the values of v_{test}/v_{pred} tend to remain relatively constant as the shear span to depth ratio increases. None of the studied specimens are in the range of small a/d values for which direct transfer of the load to the support plays a role.

Figure 21e shows that, for the Model Code 2010 [9] ACI 318-19 [7], the values of v_{test}/v_{pred} remain constant despite the increase in the absolute value of eccentricity. Nonetheless, for NEN-EN 1992-1-1:2005 [8], these values drastically decrease and become unsafe when eccentricities exceed 1000 mm. This observation can be explained by Equation (18) for most edge and corner slab–column connection entries due to the direction of the eccentricity. This equation does not consider the magnitude of the eccentricity being evaluated, just its direction; thus, for large eccentricities, this approach becomes unsafe.

4. Discussion

High-strength concrete slabs are not included in the study due to the lack of experiments on high-strength concrete slab–column connections. Future studies may investigate the behavior of this type of slabs in comparison with the ones considered in this study. Ngo [36] presented a study on concentric experiments on high-strength concrete slabs without shear reinforcement and concluded that the use of high-strength concrete improves the punching shear resistance. However, as the aggregate interlock capacity decreases for higher strength concrete, further research on this topic is warranted.

Real-scale slab–column experiments on punching shear are not commonly found in the literature. None of the entries in this database is considered a realistic size slab, as none of these has an effective depth over 200 mm. Since a size effect occurs in punching shear for concentric slab–column connections [37], experimental research on larger slabs under eccentric punching shear is necessary.

In most cases, the results found in the literature indicate that there is an important reduction in the punching capacity when unbalanced moments occur in the slab–column connection. Nevertheless, most experiments and research works focus on concentric punching shear. The code provisions are based on empirical equations, which include the effect of eccentricities by different methods, such as critical perimeter reduction or increase in the applied shear stress, but a mechanics-based model that is practical enough to be implemented in the building codes is lacking. Mechanics-based models, such as the critical shear crack theory used in the Model Code 2010 [9], are developed for the case of concentric punching shear and use simplified methods for the extension to eccentric punching shear.

For this database, the empirical methods showed large scatter in the results of the tested to predicted capacities, represented by the high coefficients of variation. This observation may be explained by the fact that all methods under consideration were originally developed for concentric punching shear and validated with concentric punching shear tests and were then extended to the use for eccentric punching shear. For the future development of design codes, more attention should be paid to eccentric punching shear and the mechanical basis of the problem. Lower bound plasticity-based models have been

shown to lead to good results in an exploratory study [38] and are a promising path toward better code models for all cases of punching shear.

5. Conclusions

The lack of understanding regarding eccentric punching shear presents a practical problem because local forces typically control the slab's design. The transfer of unbalanced moments from the slab to the column causes an increase in the resulting shear stresses. When this effect is not well understood, it may lead to a punching failure of the slab–column connection and a possible collapse of the building. This study evaluates the available code provisions against 128 experimental results reported in the literature.

Analyzing the available experimental results from the database resulted in the following conclusions:

- There is a lack of experiments on eccentric punching shear.
- All experiments are carried out on slabs of under 200 mm in depth. As such, the experiments cannot be used to evaluate the size effect in shear.
- Most specimens have large reinforcement ratios to avoid a flexural failure before reaching the punching shear capacity of the slab and are not representative of typical floor slabs.
- All specimens are cast using normal-strength concrete.

From the comparison between the experimental shear capacities and the capacities predicted by the available codes, the following conclusions result:

- The presence of unbalanced moments has a large impact on the capacity of the codes to accurately predict the performance of slab–column connections, especially for edge and corner connections.
- The closest to 1.0 average value for tested to predicted shear capacity is obtained with the Model Code 2010 [9] provisions, although the results are on the unsafe side (average of tested/predicted = 0.82).
- Evaluating all experiments, the coefficient of variation of the tested to predicted shear capacities is lower for the expressions of the Model Code 2010 [9], based on the critical shear crack theory, than for the empirical expressions of NEN-EN 1992-1-1:2005 [8] and ACI 318-19 [7].
- In general, the coefficient of variation of the tested to predicted shear capacities is lower for the experiments without shear reinforcement than for the experiments with shear reinforcement. This observation indicates that further studies should address the distribution of shear stresses for shear-reinforced slab–column connections with unbalanced moments, as well as the contribution of the various shear-carrying mechanisms for the case with shear reinforcement.
- The NEN-EN 1992-1-1:2005 [8] results for tested to predicted shear capacity showed a smaller scatter for internal and corner slab–column connections than the results of the Model Code 2010 [9] and ACI 318-19 [7].
- The Model Code 2010 [9] has the lowest coefficient of variation for the tested to predicted shear stress for edge slab–column connections, whereas NEN-EN 1992-1-1:2005 [8] has the smallest COV for internal and corner slab–column connections.
- The *fib* Model Code generally results in the best performance in the parameter studies of the tested to predicted ratios, indicating that this mechanics-based model has a better representation of the parameters than the empirical models in NEN-EN 1992-1-1:2005 [8] and ACI 318-19 [7].
- For eccentricities over 1000 mm, the use of NEN-EN 1992-1-1:2005 [8] becomes unsafe for inward eccentricities at edge slab–column connections.

From the comparison between the SCIA Engineer [33] FEM results and the predicted shear capacities for ACI 318-19 [7], the following conclusions result:

- Using a more refined calculation method to determine the acting shear stresses does not improve the results in terms of tested to predicted shear stresses when using

the ACI 318-19 [7] shear capacities. This observation indicates that the shear stress distribution that follows from a linear finite element analysis does not correspond to the slab at failure when cracking and redistribution of stresses occur.

- The ACI 318-19 [7] shear capacity should be combined with the method for determining the shear stress on the punching perimeter described in ACI 318-19 [7].
- Further research is necessary on the capacity methods that can be combined with a linear finite element analysis.

A better understanding of eccentric punching shear and further experiments on deeper slabs, slabs with high-strength concrete and carefully instrumented slabs with shear reinforcement are necessary to obtain safe designs, optimize the design of building floors and develop better tools for the assessment of existing building slabs.

Author Contributions: Conceptualization, E.O.L.L.; methodology, D.V. and E.O.L.L.; software, D.V.; validation, A.S.G. and E.O.L.L.; formal analysis, D.V.; investigation, D.V. and E.O.L.L.; resources, E.O.L.L.; data curation, D.V. and E.O.L.L.; writing—original draft preparation, D.V. and E.O.L.L.; writing—review and editing, A.S.G.; visualization, D.V.; supervision, E.O.L.L.; project administration, E.O.L.L.; funding acquisition, E.O.L.L. All authors have read and agreed to the published version of the manuscript.

Nomenclature

A_{sw}	area of the shear reinforcement for NEN-EN 1992-1-1:2005
A_v	area of the shear reinforcement for ACI 318-19
$C_{Rd,\,c}$	constant used for determining the shear capacity
E_s	modulus of elasticity of the steel
J_c	polar moment of inertia of the critical section
L_x	dimension of the slab
L_y	dimension of the slab
M_{Ed}	design moment
M_{mu}	model ultimate internal moment
M_u	factored moment applied on the slab
U_1	control perimeter for NEN-EN 1992-1-1:2005
$U_1{}^*$	reduced critical control perimeter for NEN-EN 1992-1-1:2005
V_{Ed}	design shear strength
V_{Rd}	punching resistance for Model Code 2010
$V_{Rd,c}$	punching resistance provided by the concrete for Model Code 2010
$V_{Rd,s}$	punching resistance provided by the steel for Model Code 2010
V_u	factored shear applied on the slab
V_{mu}	model ultimate internal shear
W_{sup}	width of the support
W_1	plastic modulus of control perimeter for NEN-EN 1992-1-1:2005
a	shear span
a_v	clear shear span
b_0	control perimeter for Model Code 2010
$b_{0,int}$	critical perimeter inside the shear-reinforced zone for CSCT
b_1	dimension of the critical perimeter for NEN-EN 1992-1-1:2005

$b_{1,MC}$	basic control perimeter for Model Code 2010
b_2	dimension of the critical perimeter for Model Code 2010
b_o	perimeter of the critical perimeter for ACI 318-19
b_u	diameter of the circle with the same area as the region inside $b_{1,MC}$
b_y	dimension of the critical perimeter U_1
b_z	dimension of the critical perimeter U_1
c	distance to the centroid of the critical perimeter
c_1	dimension of the column
c_2	dimension of the column
d	average effective depth of the slab
d_g	maximum aggregate size
d_v	average effective depth of the slab for Model Code 2010
e	eccentricity M/V
e_{par}	eccentricity parallel to the edge of the slab
e_u	eccentricity of the resultant forces
e_y	eccentricity caused by a moment acting on the y-axis
e_z	eccentricity caused by a moment acting on the x-axis
f_{bd}	bond strength
f_c	compressive strength of the concrete for ACI 318-19
f_{ck}	compressive strength of the concrete for Model Code 2010
f_{ct}	tensile strength of the concrete
f_{yt}	yield strength of the reinforcement
f_{ywd}	design yield strength of the shear reinforcement
$f_{ywd,ef}$	effective design strength of shear reinforcement
h	depth of the slab
k	size effect factor
k_c	column size effect factor
k_{dg}	coefficient of aggregate size
k_e	coefficient of eccentricity
k_ψ	coefficient of rotation
m_{rd}	average flexural strength per unit length in the support strip
m_{sd}	average moment per unit length for calculation of flexural reinforcement in the support strip
r_s	distance from column axis to line of contra-flexure of the radial bending moments
m_{xD}	model design moment on the x-axis
m_{yD}	model design moment on the y-axis
s_r	radial spacing of the reinforcement
v_c	punching resistance provided by the concrete for ACI 318-19
v_{Ed}	design shear stress
v_n	nominal shear strength for ACI 318-19
$v_{Rd,c}$	shear resistance provided by the concrete
v_{Rd}	shear resistance for Model Code 2010
$v_{Rd,cs}$	shear resistance for NEN-EN 1992-1-1:2005
$v_{Rd\,s}$	shear resistance provided by the steel
v_s	punching resistance provided by the steel reinforcement for ACI 318-19
v_u	maximum shear stress for ACI 318-19
v_{pred}	shear capacity predicted for all the models
v_{FEM}	maximum shear stress resulting from the FEM model
γ_f	fraction of the unbalanced moment transmitted by flexure
γ_v	fraction of the unbalanced moment transmitted by shear
α	angle between shear reinforcement and horizontal plane of the slab
α_s	constant used for determining shear capacity according to ACI 318-19
β	column dimension factor according to ACI 318-19
β_{EC}	enhancement factor for eccentric shear for NEN-EN 1992-1-1:2005
ρ_l	longitudinal steel reinforcement ratio
ρ_v	shear steel reinforcement ratio
σ_{swd}	shear reinforcement stress
ϕ_w	shear reinforcement diameter
ψ	rotation of the slab

Appendix A

Table A1. Internal slab–column connections—Slab geometry.

Reference	Name	L_x (mm)	L_x (mm)	c_1 (mm)	c_2 (mm)	h (mm)	d (mm)	a (mm)	a_v (mm)
Narayani [19]	L1	2280	2280	305	305	178	151	1026	874
	L3	2280	2280	305	305	178	151	1026	874
	L4	2280	2280	305	305	178	151	1026	874
	L5	2280	2280	305	305	178	151	1026	874
	L6	2280	2280	305	305	178	151	1026	874
	L10	2280	2280	305	305	178	151	1026	874
Krüger [2]	P16A	3000	3000	300	300	150	121	1375	1225
	P30A	3000	3000	300	300	150	121	1375	1225
	PP16B	3000	3000	300	300	150	121	1375	1225
Moe [11]	M2A	1829	1829	305	305	152	114	787	635
	M4A	1829	1829	305	305	152	114	787	635
	M2	1829	1829	305	305	152	114	787	635
	M3	1829	1829	305	305	152	114	787	635
	M6	1829	1829	254	254	152	114	787	660
	M7	1829	1829	254	254	152	114	787	660
	M8	1829	1829	254	254	152	114	787	660
	M9	1829	1829	254	254	152	114	787	660
	M10	1829	1829	254	254	152	114	787	660
Anis [21]	B.3	1524	1524	203	203	102	76	737	635
	B.4	1524	1524	203	203	102	76	737	635
	B.5	1524	1524	203	203	102	76	737	635
	B.6	1524	1524	203	203	102	76	737	635
Stamenkovic [23]	C/I/1	914	914	127	127	76	56	419	355
	C/I/2	914	914	127	127	76	56	419	355
	C/I/3	914	914	127	127	76	56	419	355
	C/I/4	914	914	127	127	76	56	419	355
	C/Ir/1	914	914	152	76	76	56	419	343
	C/Ir/2	914	914	152	76	76	56	419	343
	C/Ir/3	914	914	152	76	76	56	419	343
	C/Ir/4	914	914	152	76	76	56	419	343
Hanson [22]	A12	2134	1219	152	152	76	62	1067	991
	B16	2134	1219	152	305	76	62	1067	991
	C17	2134	1219	305	152	76	62	1067	914
Pina Ferreira [24]	S3	2500	2500	300	300	180	145	1250	1100
	S4	2500	2500	300	300	180	143	1250	1100
	S6	2500	2500	300	300	180	144	1250	1100
	S8	2500	2500	300	300	180	144	1250	1100

Table A2. Internal slab–column connections—Material properties.

Reference	Name	ρ (%)	f_y (MPa)	E_s (GPa)	f_c (MPa)	Age (Days)	f_{ct} (MPa)	d_g (mm)
	L1	1.78%	398	188	32.80	28	2.70	19.00
	L3	1.78%	398	188	33.10	28	2.66	19.00
Narayani [19]	L4	1.78%	398	188	45.80	28	3.45	19.00
	L5	1.78%	398	188	35.00	28	2.98	19.00
	L6	1.78%	398	188	42.10	28	3.07	19.00
	L10	1.78%	398	188	41.80	28	2.47	19.00
	P16A	1.30%	480	200	35.00	28	4.50	16.00
Krüger [2]	P30A	1.30%	480	200	35.00	28	4.50	16.00
	PP16B	1.30%	480	200	35.00	28	4.50	16.00
	M2A	1.50%	481	196	15.51	25	2.99	38.10
	M4A	1.50%	481	196	17.65	23	3.19	38.10
	M2	1.50%	481	196	25.72	22	3.85	38.10
	M3	1.50%	481	196	22.72	20	3.62	38.10
Moe [11]	M6	1.34%	328	196	26.48	26	3.91	38.10
	M7	1.34%	328	196	24.96	24	3.80	38.10
	M8	1.34%	328	196	24.61	24	3.77	38.10
	M9	1.34%	328	196	23.24	22	3.66	38.10
	M10	1.34%	328	196	21.10	25	3.49	38.10
	B.3	2.19%	331	205	38.06	28	4.69	9.53
Anis [21]	B.4	2.19%	331	205	37.23	28	4.64	9.53
	B.5	2.19%	331	205	36.20	28	4.57	9.53
	B.6	2.19%	331	205	39.16	28	4.76	9.53
	C/I/1	1.17%	413	192	45.02	7	5.10	9.53
	C/I/2	1.17%	413	192	37.09	7	4.63	9.53
	C/I/3	1.17%	413	192	31.92	7	4.29	9.53
Stamenkovic [23]	C/I/4	1.17%	413	192	31.37	7	4.26	9.53
	C/Ir/1	1.17%	413	192	28.27	7	4.04	9.53
	C/Ir/2	1.17%	413	192	36.54	7	4.59	9.53
	C/Ir/3	1.17%	413	192	35.71	7	4.54	9.53
	C/Ir/4	1.17%	413	192	33.23	7	4.38	9.53
	A12	1.36%	372	192	33.23	28	4.38	9.53
Hanson [22]	B16	1.36%	341	192	30.41	28	4.19	9.53
	C17	1.36%	341	192	35.99	28	4.56	9.53
	S3	1.46%	540	213	50.30	28	4.30	9.50
Pina Ferreira [24]	S4	1.48%	540	213	49.20	28	4.40	9.50
	S6	1.47%	540	213	50.10	28	4.90	9.50
	S8	1.47%	540	213	48.40	28	4.00	9.50

Table A3. Edge slab–column connections—Slab geometry.

Reference	Name	L_x (mm)	L_x (mm)	c_1 (mm)	c_2 (mm)	h (mm)	d (mm)	a (mm)	a_v (mm)
Albuquerque [17]	L1	2350	1700	300	300	180	147	2000	1850
	L2	2350	1700	300	300	180	146	2000	1850
	L3	2350	1700	300	300	180	146	2000	1850
	L4	2350	1700	300	300	180	146	2000	1850
	L5	2350	1700	300	300	180	146	2000	1850
	L6	2350	1700	300	300	180	146	2000	1850
	L7	2350	1700	300	300	180	146	2000	1850
	L8	2350	1700	300	300	180	146	2000	1850
	L9	2350	1700	300	300	180	146	2000	1850
	L10	2350	1700	300	300	180	146	2000	1850
	L11	2350	1700	300	300	180	146	2000	1850
	L12	2350	1700	300	300	180	146	2000	1850
	L13	2350	1700	300	300	180	146	2000	1850
Narayani [19]	ES1	1295	2280	305	305	178	151	1029	876
	ES2	1295	2280	305	305	178	151	1029	876
	ES3	1295	2280	305	305	178	151	1029	876
	ES4	1295	2280	305	305	178	151	1029	876
	ES5	1295	2280	305	305	178	151	1029	876
	ES6	1295	2280	305	305	178	151	1029	876
	ES7	1295	2280	305	305	178	151	1029	876
Zaghlool [20]	Z—IV (1)	965	1829	178	178	152	121	870	781
	Z—V (1)	965	1829	267	267	152	121	826	692
	Z—V (2)	965	1829	267	267	152	121	826	692
	Z—V (3)	965	1829	267	267	152	118	826	692
	Z—V (4)	965	1829	267	267	152	121	826	692
	Z—V (5)	965	1829	267	267	152	121	826	692
	Z—V (6)	965	1829	267	267	152	121	826	692
	Z—VI (1)	965	1829	356	356	152	121	781	603
Stamenkovic [23]	M(T)/E/1	914	914	127	127	76	56	812	749
	M(T)/E/2	914	914	127	127	76	56	812	749
	C(T)/E/1	914	914	127	127	76	56	812	749
	C(T)/E/2	914	914	127	127	76	56	812	749
	C(T)/E/3	914	914	127	127	76	56	812	749
	C(T)/E/4	914	914	127	127	76	56	812	749
	V/E/1	914	914	127	127	76	56	812	749
	M(II)/E/1	914	914	127	127	76	56	812	749
	C(II)/E/1	914	914	127	127	76	56	812	749
	C(II)/E/2	914	914	127	127	76	56	812	749
	C(II)/E/3	914	914	127	127	76	56	812	749
	C(II)/E/4	914	914	127	127	76	56	812	749

Table A3. *Cont.*

Reference	Name	L_x (mm)	L_x (mm)	c_1 (mm)	c_2 (mm)	h (mm)	d (mm)	a (mm)	a_v (mm)
Hanson [22]	D15	1143	1219	152	152	76	62	1067	991
Ritchie [25]	1	1350	1900	250	250	150	122	1175	1050
Sudarsana [26]	E1	711	1219	203	203	140	105	610	508
	E2	711	1219	203	203	140	105	610	508
	E4	711	1219	203	203	140	105	610	508
	E1-1	1571	1719	203	203	140	105	1220	1118
	E1-2	1571	1719	203	203	140	105	1220	1118
	E1-3	1571	1719	203	203	140	105	1220	1118
	E1-4	1571	1719	203	203	140	105	1220	1118
	E2-1	961	2940	203	203	140	105	610	508
	E2-2	961	2940	203	203	140	105	610	508
	E2-3	961	2940	203	203	140	105	610	508
	E2-4	961	2940	203	203	140	105	610	508
Zaghloul [27]	ZJESSS	1060	1770	250	250	150	119	850	725
	ZJES	1060	1770	250	250	150	119	850	725

Table A4. Edge slab–column connections—Material properties.

Reference	Name	ρ (%)	f_y (MPa)	E_s (GPa)	f_c (MPa)	Age (Days)	f_{ct} (MPa)	d_g (mm)
Albuquerque [17]	L1	1.00%	558	192	46.80	28	3.40	9.50
	L2	1.30%	558	192	44.70	28	3.00	9.50
	L3	1.30%	558	192	45.10	28	3.10	9.50
	L4	1.30%	558	192	46.00	28	3.30	9.50
	L5	1.30%	558	192	51.40	28	4.10	9.50
	L6	1.30%	558	192	52.10	28	4.30	9.50
	L7	1.50%	558	192	50.00	28	3.70	9.50
	L8	1.40%	558	192	50.50	28	3.90	9.50
	L9	1.50%	558	192	57.60	28	3.20	9.50
	L10	1.50%	558	192	59.30	28	3.60	9.50
	L11	1.50%	558	192	43.10	28	3.10	9.50
	L12	1.50%	558	192	43.60	28	3.30	9.50
	L13	1.50%	558	192	44.10	28	3.40	9.50
Narayani [19]	ES1	0.88%	398	188	33.80	28	2.70	19.00
	ES2	0.88%	398	188	32.80	28	2.70	19.00
	ES3	0.88%	398	188	51.30	28	3.10	19.00
	ES4	0.88%	398	188	50.00	28	3.31	19.00
	ES5	0.88%	398	188	37.60	28	2.63	19.00
	ES6	0.88%	398	188	40.40	28	2.23	19.00
	ES7	0.88%	398	188	45.80	28	3.38	19.00

Table A4. *Cont.*

Reference	Name	ρ (%)	f_y (MPa)	E_s (GPa)	f_c (MPa)	Age (Days)	f_{ct} (MPa)	d_g (mm)
Zaghlool [20]	Z—IV (1)	1.23%	476	207	27.34	28	2.99	19.05
	Z—V (1)	1.23%	474	207	34.34	28	3.52	19.05
	Z—V (2)	1.65%	474	207	40.47	28	3.61	19.05
	Z—V (3)	2.23%	475	207	38.75	28	3.79	19.05
	Z—V (4)	1.23%	475	207	35.03	28	4.10	19.05
	Z—V (5)	1.23%	476	207	35.16	28	3.58	19.05
	Z—V (6)	1.23%	476	207	31.30	28	3.63	19.05
	Z—VI (1)	1.23%	476	207	25.99	28	2.83	19.05
Stamenkovic [23]	M(T)/E/1	1.17%	413	192	30.34	7	4.19	9.53
	M(T)/E/2	1.17%	413	192	33.09	7	4.37	9.53
	C(T)/E/1	1.17%	413	192	38.47	7	4.71	9.53
	C(T)/E/2	1.17%	413	192	32.41	7	4.33	9.53
	C(T)/E/3	1.17%	413	192	33.99	7	4.43	9.53
	C(T)/E/4	1.17%	413	192	34.34	7	4.45	9.53
	V/E/1	1.17%	413	192	35.85	7	4.55	9.53
	M(II)/E/1	1.17%	413	192	36.20	7	4.57	9.53
	C(II)/E/1	1.17%	413	192	34.82	7	4.48	9.53
	C(II)/E/2	1.17%	413	192	35.51	7	4.53	9.53
	C(II)/E/3	1.17%	413	192	34.89	7	4.49	9.53
	C(II)/E/4	1.17%	413	192	36.54	7	4.59	9.53
Hanson [22]	D15	1.15%	365	192	31.10	28	4.24	9.53
Ritchie [25]	1	1.12%	432	192	26.20	28	3.89	9.50
Sudarsana [26]	E1	0.90%	420	183	43.62	28	5.02	10.00
	E2	0.90%	420	183	42.41	28	4.95	10.00
	E4	0.90%	420	183	43.62	28	5.02	10.00
	E1-1	1.60%	420	183	52.80	28	5.52	10.00
	E1-2	1.60%	420	183	52.80	28	5.52	10.00
	E1-3	1.60%	420	183	55.00	28	5.64	10.00
	E1-4	1.60%	420	183	52.80	28	5.52	10.00
	E2-1	0.80%	420	183	52.80	28	5.52	10.00
	E2-2	0.80%	420	183	52.80	28	5.52	10.00
	E2-3	0.80%	420	183	55.00	28	5.64	10.00
	E2-4	0.80%	420	183	55.00	28	5.64	10.00
Zaghloul [27]	ZJESSS	1.40%	400	192	42.00	28	4.93	10.00
	ZJES	1.40%	400	192	42.00	28	4.93	10.00

Table A5. Corner slab–column connections—Slab geometry.

Reference	Name	L_x (mm)	L_x (mm)	c_1 (mm)	c_2 (mm)	h (mm)	d (mm)	a (mm)	a_v (mm)
Zaghlool [20]	Z—I (1)	1067	1067	178	178	152	121	965	1067
	Z—II (1)	1067	1067	267	267	152	121	921	1067
	Z—II (2)	1067	1067	267	267	152	121	921	1067
	Z—II (3)	1067	1067	267	267	152	118	921	1067
	Z—II (4)	1067	1067	267	267	152	121	921	1067
	Z—II (6)	1067	1067	267	267	152	121	921	1067
	Z—III (1)	1067	1067	356	356	152	121	876	1067
Sudarsana [26]	C5	711	711	305	305	140	105	559	711
	C6	711	711	305	305	140	105	559	711
	C7	711	711	305	305	140	105	559	711
	C8	711	711	305	305	140	105	559	711
Desayi [28]	S101	530	530	100	100	100	80	480	530
	S201	530	530	100	100	100	80	480	530
	S301	530	530	100	100	100	80	480	530
	S102	530	530	100	100	100	80	480	530
	S202	530	530	100	100	100	80	480	530
	S302	530	530	100	100	100	80	480	530
Walker [29]	SC1	1525	1525	300	300	125	100	1375	1525
	SC2	1525	1525	300	300	125	100	1375	1525
	SC3	1525	1525	300	300	125	100	1375	1525
	SC4	1525	1525	220	220	125	100	1415	1525
	SC5	1525	1525	220	220	125	100	1415	1525
	SC7	1525	1525	220	220	125	100	1415	1525
	SC8	1000	1000	160	160	80	64	920	1000
	SC9	1000	1000	160	160	80	64	920	1000
	SC11	1000	700	160	160	80	60	920	1000
	SC12	1000	700	300	300	80	60	850	1000
Stamenkovic [30]	C/C/1	914	914	127	127	76	56	813	914
	C/C/2	914	914	127	127	76	56	813	914
	C/C/3	914	914	127	127	76	56	813	914
	C/C/4	914	914	127	127	76	56	813	914
Ghali [18]	NH1	1075	1075	250	250	150	114	910	1075
	NH2	1075	1075	250	250	150	114	910	1075
	NH3	1075	1075	250	250	150	114	910	1075
	NH4	1075	1075	250	250	150	114	910	1075
	NH5	1075	1075	250	250	150	114	910	1075

Table A6. Corner slab–column connections—Material description.

Reference	Name	ρ (%)	f_y (MPa)	E_s (GPa)	f_c (MPa)	Age (Days)	f_{ct} (MPa)	d_g (mm)
Zaghlool [20]	Z—I (1)	1.23%	379	207	32.68	28	4.34	19.05
	Z—II (1)	1.23%	389	207	33.03	28	4.37	19.05
	Z—II (2)	1.65%	405	207	33.44	28	4.39	19.05
	Z—II (3)	2.23%	451	207	27.72	28	4.00	19.05
	Z—II (4)	1.23%	389	207	30.75	28	4.21	19.05
	Z—II (6)	1.23%	381	207	33.58	28	4.40	19.05
	Z—III (1)	1.23%	379	207	33.65	28	4.41	19.05
Sudarsana [26]	C5	1.11%	420	183	44.40	28	5.06	10.00
	C6	1.11%	420	183	44.40	28	5.06	10.00
	C7	1.11%	420	183	44.40	28	5.06	10.00
	C8	1.11%	420	183	44.40	28	5.06	10.00
Desayi [28]	S101	0.53%	720	192	45.00	28	5.10	9.50
	S201	0.80%	720	192	45.00	28	5.10	9.50
	S301	1.07%	720	192	25.00	28	3.80	9.50
	S102	0.53%	720	192	31.00	28	4.23	9.50
	S202	0.80%	720	192	34.00	28	4.43	9.50
	S302	1.07%	720	192	28.00	28	4.02	9.50
Walker [29]	SC1	1.14%	595	192	43.30	28	5.00	20.00
	SC2	1.11%	595	192	47.90	28	5.26	20.00
	SC3	1.13%	595	192	37.40	28	4.65	20.00
	SC4	1.14%	595	192	40.80	28	4.85	20.00
	SC5	1.71%	595	192	46.50	28	5.18	20.00
	SC7	1.71%	595	192	43.80	28	5.03	20.00
	SC8	1.37%	595	192	37.40	28	4.65	20.00
	SC9	1.24%	595	192	34.30	28	4.45	20.00
	SC11	1.27%	595	192	27.20	28	3.96	20.00
	SC12	1.18%	595	192	40.70	28	4.85	20.00
Stamenkovic [30]	C/C/1	1.17%	413	192	38.06	28	4.69	9.50
	C/C/2	1.17%	413	192	35.37	28	4.52	9.50
	C/C/3	1.17%	413	192	32.27	28	4.32	9.50
	C/C/4	1.17%	413	192	38.27	28	4.70	9.50
Ghali [18]	NH1	1.45%	440	200	41.50	28	4.90	9.50
	NH2	1.45%	440	200	42.20	28	4.94	9.50
	NH3	1.45%	440	200	36.40	28	4.59	9.50
	NH4	1.45%	440	200	36.90	28	4.62	9.50
	NH5	1.45%	440	200	33.20	28	4.38	9.50

Table A7. Database—Shear reinforcement.

Reference	Name	Type	f_y (MPa)	E_s (GPa)	Φ_w (mm)	s (mm)
Narayani [19]	L3	Shear hats	309.00	207.00	9.50	90.00
	L4	Shear hats	238.00	207.00	6.50	90.00
	L5	Shear hats	355.00	207.00	13.00	90.00
	L6	Shear hats	355.00	207.00	8.00	90.00
	L10	Shear hats	355.00	207.00	8.00	90.00
Krüger [2]	PP16B	Stirrups	480.00	200.00	10.00	120.00
Pina Ferreira [24]	S3	Shear studs	535.00	211.00	10.00	100.00
	S4	Shear studs	535.00	211.00	10.00	100.00
	S8	Shear studs	518.00	204.00	12.00	100.00
Albuquerque [17]	L9	Shear heads	587.00	188.00	8.00	100.00
	L10	Shear heads	587.00	188.00	8.00	100.00
	ES3	Stirrups	238.00	207.00	6.50	70.00
	ES4	Stirrups	309.00	207.00	9.50	70.00
	ES6	Stirrups	238.00	207.00	6.50	70.00
	ES7	Stirrups	238.00	207.00	6.50	70.00
Zaghloul [27]	ZJESSS	Shear stud	345.00	192.00	12.70	90.00
Ghali [18]	NH3	Shear heads	440.00	200.00	6.00	57.00
	NH5	Shear heads	440.00	200.00	6.00	85.00

Figure 12 illustrates the "Shear Hats" type of shear reinforcement.

Appendix B

Table A8. Internal slab–column connections—Tested to predicted shear capacity.

Reference	Name	ACI [7]			EC2 [8]			MC 2010 [9]		
		Test (MPa)	Pred (MPa)	Test/Pred	Test (MPa)	Pred (MPa)	Test/Pred	Test (MPa)	Pred (MPa)	Test/Pred
Narayani [19]	L1	2.58	1.89	1.37	1.34	1.40	0.96	2.49	3.44	0.73
	L3	3.23	2.98	1.08	1.68	1.34	1.25	1.23	1.40	0.88
	L4	3.67	2.25	1.63	1.91	1.50	1.28	1.40	1.62	0.87
	L5	3.23	4.41	0.73	1.68	1.37	1.23	1.23	1.46	0.84
	L6	3.02	2.88	1.05	1.64	1.45	1.13	1.48	1.92	0.77
	L10	3.22	2.87	1.12	1.75	1.45	1.21	1.57	1.92	0.82
Krüger [2]	P16A	2.51	1.95	1.28	1.46	1.29	1.13	2.54	3.47	0.73
	P30A	2.67	1.95	1.37	1.49	1.29	1.16	2.65	3.49	0.76
	PP16B	3.22	3.41	0.95	1.87	2.73	0.69	0.61	0.75	0.82
Moe [11]	M2A	1.75	1.30	1.35	1.03	1.03	1.00	1.74	2.36	0.74
	M4A	1.73	1.39	1.25	0.98	1.07	0.91	1.66	2.52	0.66
	M2	2.43	1.67	1.45	1.43	1.22	1.17	2.39	3.04	0.79
	M3	2.17	1.57	1.38	1.24	1.17	1.06	2.09	2.86	0.73
	M6	2.25	1.70	1.33	1.25	1.18	1.05	2.25	3.09	0.73
	M7	2.28	1.65	1.38	1.32	1.16	1.14	2.36	3.00	0.79
	M8	2.19	1.64	1.34	1.14	1.15	0.99	2.12	2.98	0.71
	M9	2.30	1.59	1.44	1.29	1.13	1.14	2.32	2.89	0.80
	M10	2.16	1.52	1.43	1.15	1.10	1.05	2.11	2.76	0.77

Table A8. *Cont.*

Reference	Name	ACI [7]			EC2 [8]			MC 2010 [9]		
		Test (MPa)	Pred (MPa)	Test/Pred	Test (MPa)	Pred (MPa)	Test/Pred	Test (MPa)	Pred (MPa)	Test/Pred
Anis [21]	B.3	3.20	2.04	1.57	1.91	1.53	1.25	3.17	3.70	0.86
	B.4	3.01	2.01	1.49	1.74	1.51	1.15	2.86	3.66	0.78
	B.5	3.48	1.99	1.75	1.95	1.50	1.30	3.20	3.61	0.89
	B.6	4.08	2.07	1.98	2.24	1.54	1.46	3.65	3.75	0.97
Stamenkovic [23]	C/I/1	3.25	2.21	1.47	1.81	1.35	1.34	3.19	4.03	0.79
	C/I/2	3.20	2.01	1.59	1.71	1.27	1.35	3.01	3.65	0.82
	C/I/3	3.00	1.86	1.61	1.52	1.20	1.26	2.67	3.39	0.79
	C/I/4	3.16	1.85	1.71	1.55	1.20	1.29	2.72	3.36	0.81
	C/Ir/1	3.68	1.75	2.10	1.98	1.16	1.72	3.58	3.09	1.16
	C/Ir/2	3.87	1.99	1.94	2.01	1.26	1.60	3.61	3.63	0.99
	C/Ir/3	1.92	1.97	0.98	1.02	1.25	0.82	1.85	3.59	0.51
	C/Ir/4	1.65	1.90	0.87	0.84	1.22	0.69	1.50	3.46	0.43
Hanson [22]	A12	2.64	1.90	1.39	1.35	1.28	1.06	2.63	3.46	0.76
	B16	2.21	1.82	1.22	1.12	1.24	0.90	1.98	3.31	0.60
	C17	1.94	1.98	0.98	1.21	1.32	0.92	1.81	3.60	0.50
Pina Ferreira [24]	S3	4.63	3.16	1.47	2.45	1.72	1.42	1.87	1.74	1.08
	S4	4.83	2.70	1.79	2.57	2.34	1.10	1.33	1.18	1.13
	S6	3.52	2.34	1.51	1.86	1.51	1.23	3.50	3.95	0.89
	S8	5.62	3.05	1.84	3.03	2.32	1.31	1.71	1.42	1.21

Table A9. Edge slab–column connections—Tested to predicted shear capacity.

Reference	Name	ACI [7]			EC2 [8]			MC 2010 [9]		
		Test (MPa)	Pred (MPa)	Test/Pred	Test (MPa)	Pred (MPa)	Test/Pred	Test (MPa)	Pred (MPa)	Test/Pred
Albuquerque [17]	L1	2.66	2.26	1.18	1.65	1.30	1.27	3.07	3.49	0.88
	L2	2.94	2.21	1.33	2.52	1.39	1.81	1.91	3.80	0.50
	L3	4.98	2.22	2.25	3.14	1.40	2.24	2.57	4.03	0.64
	L4	4.80	2.24	2.14	2.87	1.41	2.04	2.39	4.07	0.59
	L5	4.75	2.37	2.01	3.52	1.46	2.41	2.76	3.99	0.69
	L6	5.31	2.38	2.23	3.58	1.47	2.44	2.88	4.19	0.69
	L7	6.58	2.33	2.82	3.94	1.52	2.60	3.28	4.24	0.77
	L8	7.31	2.35	3.12	4.38	1.49	2.94	3.64	4.26	0.85
	L9	4.57	2.72	1.68	3.91	2.59	1.51	1.34	1.93	0.69
	L10	7.16	2.75	2.60	4.82	2.61	1.85	1.22	1.41	0.86
	L11	6.62	2.17	3.06	4.06	1.44	2.81	3.35	3.94	0.85
	L12	5.24	2.18	2.41	3.69	1.45	2.54	2.93	3.81	0.77
	L13	7.55	2.19	3.45	4.63	1.46	3.18	3.82	3.95	0.97
Narayani [19]	ES1	2.83	1.92	1.48	2.95	1.12	2.64	2.36	3.42	0.69
	ES2	2.02	1.89	1.07	1.74	1.11	1.57	2.29	3.27	0.70
	ES3	2.61	1.61	1.62	1.88	1.14	1.65	1.80	2.43	0.74
	ES4	3.00	2.29	1.31	2.16	1.13	1.92	2.07	2.42	0.85
	ES5	3.28	2.02	1.62	3.31	1.16	2.86	2.76	3.68	0.75
	ES6	3.39	1.47	2.30	3.53	1.05	3.37	1.51	1.98	0.76
	ES7	3.85	1.54	2.50	3.88	1.09	3.55	1.26	1.59	0.79

Table A9. *Cont.*

Reference	Name	ACI [7]			EC2 [8]			MC 2010 [9]		
		Test (MPa)	Pred (MPa)	Test/Pred	Test (MPa)	Pred (MPa)	Test/Pred	Test (MPa)	Pred (MPa)	Test/Pred
Zaghlool [20]	Z—IV (1)	2.91	1.73	1.69	1.06	1.16	0.91	3.24	3.14	1.03
	Z—V (1)	2.93	1.93	1.51	0.98	1.25	0.78	2.83	3.52	0.81
	Z—V (2)	3.72	2.10	1.77	1.91	1.46	1.31	4.03	3.82	1.06
	Z—V (3)	4.24	2.05	2.07	2.17	1.53	1.41	4.57	3.73	1.22
	Z—V (4)	4.38	1.95	2.24	-	-	-	-	-	-
	Z—V (5)	3.59	1.96	1.84	3.13	1.26	2.48	2.34	3.56	0.66
	Z—V (6)	3.24	1.85	1.75	0.91	1.22	0.75	2.83	3.36	0.84
	Z—VI (1)	2.95	1.68	1.75	1.86	1.14	1.63	3.16	3.06	1.03
Stamenkovic [23]	M(T)/E/1	4.43	1.82	2.44	-	-	-	-	-	-
	M(T)/E/2	4.35	1.90	2.29	-	-	-	-	-	-
	C(T)/E/1	3.25	2.05	1.59	2.62	1.28	2.04	3.92	3.39	1.16
	C(T)/E/2	3.62	1.88	1.93	1.96	1.21	1.62	3.94	3.30	1.20
	C(T)/E/3	3.77	1.92	1.96	0.89	1.23	0.73	2.98	3.50	0.85
	C(T)/E/4	3.95	1.93	2.05	0.39	1.23	0.32	2.21	3.52	0.63
	V/E/1	4.37	1.98	2.21	3.84	1.25	3.07	2.85	3.33	0.86
	M(II)/E/1	2.64	1.99	1.33	-	-	-	-	-	-
	C(II)/E/1	3.74	1.95	1.92	1.64	1.24	1.32	2.73	3.53	0.77
	C(II)/E/2	3.28	1.97	1.67	1.25	1.25	1.00	2.48	3.58	0.69
	C(II)/E/3	3.42	1.95	1.76	0.84	1.24	0.68	2.79	3.54	0.79
	C(II)/E/4	2.96	1.99	1.48	0.46	1.26	0.37	2.54	3.63	0.70
Hanson [22]	D15	3.89	1.84	2.11	0.34	1.19	0.29	1.80	3.35	0.54
Ritchie [25]	1	1.61	1.69	0.95	1.10	1.11	0.99	1.35	3.07	0.44
Sudarsana [26]	E1	2.60	2.18	1.19	1.36	1.22	1.11	2.92	3.96	0.74
	E2	4.18	2.15	1.94	3.53	1.21	2.91	2.71	3.73	0.73
	E4	1.61	2.18	0.74	1.24	1.22	1.01	1.99	3.96	0.50
	E1-1	1.13	2.40	0.47	0.85	1.58	0.54	1.13	4.36	0.26
	E1-2	3.26	2.40	1.36	0.94	1.58	0.59	3.04	4.36	0.70
	E1-3	3.99	2.45	1.63	3.27	1.60	2.04	5.04	3.73	1.35
	E1-4	2.79	2.40	1.16	1.21	1.58	0.77	3.02	4.36	0.69
	E2-1	2.64	2.40	1.10	1.39	1.25	1.11	2.97	4.36	0.68
	E2-2	2.62	2.40	1.09	1.90	1.25	1.52	3.19	4.31	0.74
	E2-3	5.28	2.45	2.16	3.49	1.27	2.75	4.41	3.86	1.14
	E2-4	2.39	2.45	0.98	2.12	1.27	1.67	3.10	4.35	0.71
Zaghloul [27]	ZJESSS	4.93	4.02	1.23	1.76	2.02	0.87	1.21	1.07	1.13
	ZJES	2.52	2.14	1.18	1.52	1.40	1.09	2.87	3.89	0.74

Table A10. Corner slab–column connections—Tested to predicted shear capacity.

Reference	Name	ACI [7]			EC2 [8]			MC 2010 [9]		
		Test (MPa)	Pred (MPa)	Test/Pred	Test (MPa)	Pred (MPa)	Test/Pred	Test (MPa)	Pred (MPa)	Test/Pred
Zaghlool [20]	Z—I (1)	2.89	1.89	1.53	1.46	1.23	1.18	2.69	3.43	0.78
	Z—II (1)	3.38	1.90	1.78	2.50	1.24	2.02	3.20	3.45	0.93
	Z—II (2)	4.62	1.91	2.42	3.21	1.37	2.34	4.26	3.47	1.23
	Z—II (3)	5.13	1.74	2.95	3.38	1.37	2.46	4.57	3.16	1.45
	Z—II (4)	2.00	1.83	1.09	-	-	-	-	-	-
	Z—II (6)	3.14	1.91	1.64	1.49	1.24	1.20	2.48	3.48	0.71
	Z—III (1)	3.06	1.91	1.60	3.01	1.25	2.42	3.01	3.48	0.86
Sudarsana [26]	C5	1.69	2.20	0.77	1.38	1.32	1.04	1.52	4.00	0.38
	C6	2.99	2.20	1.36	2.41	1.32	1.83	2.68	4.00	0.67
	C7	2.78	2.20	1.26	2.08	1.32	1.58	2.41	4.00	0.60
	C8	2.42	2.20	1.10	2.18	1.32	1.65	2.29	4.00	0.57
Desayi [28]	S101	3.86	2.21	1.74	1.49	1.04	1.44	3.44	4.02	0.86
	S201	5.56	2.21	2.51	2.15	1.19	1.81	4.96	4.02	1.23
	S301	6.52	1.65	3.95	2.52	1.08	2.34	5.82	3.00	1.94
	S102	4.87	1.84	2.65	2.39	0.92	2.61	4.78	3.34	1.43
	S202	3.80	1.92	1.98	1.86	1.08	1.72	3.73	3.50	1.07
	S302	3.99	1.75	2.29	1.95	1.12	1.75	3.92	3.17	1.23
Walker [29]	SC1	2.38	2.17	1.10	1.98	1.32	1.49	2.14	3.95	0.54
	SC2	2.25	2.28	0.99	1.81	1.35	1.34	2.00	4.15	0.48
	SC3	2.82	2.02	1.40	1.80	1.25	1.44	2.28	3.67	0.62
	SC4	2.53	2.11	1.20	1.69	1.30	1.30	2.29	3.83	0.60
	SC5	2.92	2.25	1.30	2.17	1.55	1.40	2.78	4.09	0.68
	SC7	4.02	2.18	1.84	2.17	1.52	1.43	3.34	3.97	0.84
	SC8	2.35	2.02	1.16	2.06	1.34	1.54	2.31	3.67	0.63
	SC9	2.82	1.93	1.46	2.06	1.26	1.64	2.55	3.51	0.72
	SC11	2.02	1.72	1.17	2.30	1.17	1.96	2.47	3.13	0.79
	SC12	1.97	2.02	0.98	3.56	1.31	2.72	1.83	3.83	0.48
Stamenkovic [30]	C/C/1	2.67	2.04	1.31	2.09	1.28	1.64	3.65	3.70	0.99
	C/C/2	2.52	1.96	1.28	1.34	1.25	1.07	3.16	3.57	0.88
	C/C/3	2.27	1.87	1.21	0.67	1.21	0.55	2.61	3.41	0.77
	C/C/4	1.99	2.04	0.98	0.30	1.28	0.24	2.16	3.71	0.58
Ghali [18]	NH1	4.43	2.13	2.08	2.99	1.41	2.12	4.04	3.87	1.05
	NH2	4.15	2.14	1.94	2.83	1.42	2.00	3.80	3.90	0.98
	NH3	4.28	2.58	1.66	2.98	2.13	1.40	1.58	1.48	1.07
	NH4	2.79	2.00	1.39	-	-	-	-	-	-
	NH5	5.69	1.95	2.93	3.64	2.01	1.82	1.35	0.94	1.44

Table A11. Internal slab–column connections—SCIA (FEM) [33] results compared with shear stress according to ACI 318-19, Equation (1), and capacity results for ACI 319-19 [7].

Reference	Name	ACI [7]			SCIA (FEM) [33]	
		Pred (MPa)	Tested (MPa)	Result (MPa)	FEM Result/Pred	Tested/FEM Result
Narayani [19]	L1	1.89	2.58	4.24	2.24	0.61
	L3	2.98	3.23	2.48	0.83	1.30
	L4	2.25	3.67	2.83	1.26	1.30
	L5	4.41	3.23	2.48	0.56	1.30
	L6	2.88	3.02	2.33	0.81	1.30
	L10	2.87	3.22	2.48	0.86	1.30
Krüger [2]	P16A	1.95	2.51	2.90	1.49	0.86
	P30A	1.95	2.67	2.96	1.51	0.90
	PP16B	3.41	3.22	3.77	1.11	0.85
Moe [11]	M2A	1.30	1.75	2.54	1.95	0.69
	M4A	1.39	1.73	2.89	2.09	0.60
	M2	1.67	2.43	3.58	2.14	0.68
	M3	1.57	2.17	3.51	2.23	0.62
	M6	1.70	2.25	3.23	1.90	0.70
	M7	1.65	2.28	2.84	1.72	0.80
	M8	1.64	2.19	3.66	2.24	0.60
	M9	1.59	2.30	3.15	1.98	0.73
	M10	1.52	2.16	3.42	2.26	0.63
Anis [21]	B.3	2.04	3.20	3.80	1.87	0.84
	B.4	2.01	3.01	3.28	1.63	0.92
	B.5	1.99	3.48	3.77	1.90	0.92
	B.6	2.07	4.08	4.47	2.17	0.91
Stamenkovic [23]	C/I/1	2.21	3.25	3.92	1.77	0.83
	C/I/2	2.01	3.20	3.91	1.95	0.82
	C/I/3	1.86	3.00	3.72	2.00	0.81
	C/I/4	1.85	3.16	3.96	2.14	0.80
	C/Ir/1	1.75	3.68	3.20	1.83	1.15
	C/Ir/2	1.99	3.87	3.31	1.66	1.17
	C/Ir/3	1.97	1.92	1.64	0.83	1.17
	C/Ir/4	1.90	1.65	1.37	0.72	1.20

Table A12. Edge slab–column connections—SCIA (FEM) [33] results compared with shear stress according to ACI 318-19, Equation (1), and capacity results for ACI 319-19 [7].

Reference	Name	ACI [7]			SCIA (FEM) [33]	
		Pred (MPa)	Tested (MPa)	Result (MPa)	FEM Result/Pred	Tested/FEM Result
Hanson [22]	A12	1.90	2.64	3.40	1.79	0.78
	B16	1.82	2.21	4.53	2.49	0.49
	C17	1.98	1.94	2.70	1.37	0.72
Pina Ferreira [24]	S3	3.16	4.63	2.13	0.67	2.17
	S4	2.70	4.83	1.88	0.70	2.57
	S6	2.34	3.52	12.76	5.46	0.28
	S8	3.05	5.62	2.41	0.79	2.33
Albuquerque [17]	L1	2.26	2.66	2.59	1.15	1.03
	L2	2.21	2.94	2.50	1.13	1.18
	L3	2.22	4.98	2.92	1.32	1.71
	L4	2.24	4.80	2.70	1.21	1.78
	L5	2.37	4.75	3.33	1.41	1.43
	L6	2.38	5.31	3.33	1.40	1.60
	L7	2.33	6.58	3.67	1.57	1.79
	L8	2.35	7.31	4.07	1.74	1.80
	L9	2.72	4.57	2.59	0.95	1.76
	L10	2.75	7.16	2.77	1.01	2.58
	L11	2.17	6.62	3.77	1.74	1.76
	L12	2.18	5.24	3.46	1.59	1.51
	L13	2.19	7.55	4.28	1.95	1.76
Narayani [19]	ES1	1.92	2.83	2.68	1.40	1.06
	ES2	1.89	2.02	2.23	1.18	0.91
	ES3	1.61	2.61	1.37	0.85	1.91
	ES4	2.29	3.00	1.56	0.68	1.92
	ES5	2.02	3.28	3.01	1.49	1.09
	ES6	1.47	3.39	1.61	1.09	2.11
	ES7	1.54	3.85	2.02	1.31	1.91
Zaghlool [20]	Z—IV (1)	1.73	2.91	1.71	0.99	1.70
	Z—V (1)	1.93	2.93	1.85	0.96	1.58
	Z—V (2)	2.10	3.72	2.13	1.02	1.74
	Z—V (3)	2.05	4.24	3.67	1.79	1.16
	Z—V (4)	1.95	4.38	1.20	0.61	3.66
	Z—V (5)	1.96	3.59	2.99	1.53	1.20
	Z—V (6)	1.85	3.24	1.56	0.85	2.07
	Z—VI (1)	1.68	2.95	4.30	2.56	0.69
Stamenkovic [23]	M(T)/E/1	1.82	4.43	3.41	1.87	1.30
	M(T)/E/2	1.90	4.35	3.34	1.76	1.30
	C(T)/E/1	2.05	3.25	2.92	1.43	1.11
	C(T)/E/2	1.88	3.62	3.87	2.06	0.93
	C(T)/E/3	1.92	3.77	4.11	2.14	0.92
	C(T)/E/4	1.93	3.95	3.57	1.85	1.11
	V/E/1	1.98	4.37	4.22	2.13	1.04
	M(II)/E/1	1.99	2.64	3.20	1.61	0.82
	C(II)/E/1	1.95	3.74	6.91	3.55	0.54
	C(II)/E/2	1.97	3.28	5.63	2.86	0.58
	C(II)/E/3	1.95	3.42	5.78	2.97	0.59
	C(II)/E/4	1.99	2.96	4.26	2.14	0.70

Table A12. *Cont.*

Reference	Name	ACI [7]			SCIA (FEM) [33]	
		Pred (MPa)	Tested (MPa)	Result (MPa)	FEM Result/Pred	Tested/FEM Result
Hanson [22]	D15	1.84	3.89	1.67	0.91	2.32
Ritchie [25]	1	1.69	1.61	1.35	0.80	1.19
Sudarsana [26]	E1	2.18	2.60	5.02	2.30	0.52
	E2	2.15	4.18	2.53	1.18	1.65
	E4	2.18	1.61	2.37	1.09	0.68
	E1-1	2.40	1.13	0.83	0.35	1.36
	E1-2	2.40	3.26	6.63	2.76	0.49
	E1-3	2.45	3.99	5.29	2.16	0.75
	E1-4	2.40	2.79	5.64	2.35	0.50
	E2-1	2.40	2.64	5.19	2.16	0.51
	E2-2	2.40	2.62	4.37	1.82	0.60
	E2-3	2.45	5.28	3.57	1.46	1.48
	E2-4	2.45	2.39	3.18	1.30	0.75
Zaghloul [27]	ZJESSS	4.02	4.93	2.20	0.55	2.24
	ZJES	2.14	2.52	4.80	2.24	0.52

Table A13. Corner slab–column connections—SCIA (FEM) [33] results compared with shear stress according to ACI 318-19, Equation (1), and capacity results for ACI 319-19 [7].

Reference	Name	ACI [7]			SCIA (FEM) [33]	
		Pred (MPa)	Tested (MPa)	Result (MPa)	FEM Result/Pred	Tested/FEM Result
Zaghlool [20]	Z—I (1)	1.89	2.89	1.83	0.97	1.58
	Z—II (1)	1.90	3.38	3.77	1.99	0.90
	Z—II (2)	1.91	4.62	4.28	2.24	1.08
	Z—II (3)	1.74	5.13	4.13	2.38	1.24
	Z—II (4)	1.83	2.00	4.03	2.20	0.49
	Z—II (6)	1.91	3.14	2.16	1.13	1.45
	Z—III (1)	1.91	3.06	5.08	2.65	0.60
Sudarsana [26]	C5	2.20	1.69	2.44	1.11	0.69
	C6	2.20	2.99	4.32	1.96	0.69
	C7	2.20	2.78	4.21	1.91	0.66
	C8	2.20	2.42	3.59	1.63	0.68
Desayi [28]	S101	2.21	3.86	3.72	1.68	1.04
	S201	2.21	5.56	5.36	2.42	1.04
	S301	1.65	6.52	6.29	3.81	1.04
	S102	1.84	4.87	7.89	4.29	0.62
	S202	1.92	3.80	6.16	3.20	0.62
	S302	1.75	3.99	6.46	3.70	0.62

Table A13. *Cont.*

Reference	Name	ACI [7]			SCIA (FEM) [33]	
		Pred (MPa)	Tested (MPa)	Result (MPa)	FEM Result/Pred	Tested/FEM Result
Walker [29]	SC1	2.17	2.38	3.88	1.79	0.61
	SC2	2.28	2.25	3.56	1.56	0.63
	SC3	2.02	2.82	3.53	1.75	0.80
	SC4	2.11	2.53	2.70	1.28	0.94
	SC5	2.25	2.92	3.49	1.55	0.84
	SC7	2.18	4.02	3.49	1.60	1.15
	SC8	2.02	2.35	5.06	2.50	0.47
	SC9	1.93	2.82	5.06	2.62	0.56
	SC11	1.72	2.02	5.23	3.04	0.39
	SC12	2.02	1.97	3.61	1.79	0.55
Stamenkovic [30]	C/C/1	2.04	2.67	6.69	3.29	0.40
	C/C/2	1.96	2.52	6.13	3.12	0.41
	C/C/3	1.87	2.27	5.37	2.87	0.42
	C/C/4	2.04	1.99	4.66	2.28	0.43
Ghali [18]	NH1	2.13	4.43	3.59	1.69	1.24
	NH2	2.14	4.15	1.39	0.65	2.99
	NH3	2.58	4.28	7.72	2.99	0.55
	NH4	2.00	2.79	5.36	2.67	0.52
	NH5	1.95	5.69	8.91	4.58	0.64

References

1. Wight, J.; MacGregor, J. Analysis, and Design. In *Reinforced Concrete Mechanics & Design*, 6th ed.; Pearson: London, UK, 2010; Volume 1.
2. Krüger, G. *Résistance au Poinçonnement Excentré des Planchers-Dalles*; EPFL: Écublens, Switzerland, 1999.
3. Muttoni, A.; Ruiz, M.F.; Simões, J.T. The theoretical principles of the critical shear crack theory for punching shear failures and derivation of consistent closed-form design expressions. *Struct. Concr.* **2018**, *19*, 174–190. [CrossRef]
4. Mirzaei, Y. Post punching behaviour of reinforced concrete slab-column connections. In Proceedings of the 7th International FIB PhD Symposium, Stuttgart, Germany, 11–13 September 2008.
5. Kinnunen, S.; Nylander, H. Punching of concrete slabs without shear reinforcement. *Elander* **1960**, *158*, 112.
6. Muttoni, A.; Ruiz, M.F. The levels-of-approximation approach in MC 2010: Application to punching shear provisions. *Struct. Concr.* **2012**, *13*, 32–41. [CrossRef]
7. ACI Committee 318. *ACI CODE-318-19: Building Code Requirements for Structural Concrete and Commentary*; American Concrete Institute: Farmington Hills, MI, USA, 2019.
8. European Committee for Standardization and British Standards Institution. *Eurocode 2: Design of Concrete Structures*; British Standards Institution: London, UK, 2005.
9. The International Federation for Structural Concrete. *fib Bulletin 55. Model Code 2010 First Complete Draft*; fib: Lausanne, Switzerland, 2010; Volume 1. [CrossRef]
10. Park, H.; Choi, K. Improved Strength Model for Interior Flat Plate-Column Connections Subject to Unbalanced Moment. *ASCE J. Struct. Eng.* **2006**, *694*, 694–704. [CrossRef]
11. Moe, J. *Shearing Strength of Reinforced Concrete Slabs and Footings under Concentrated Loads*; Development Department Bulletin No. D47; Portland Cement Association: Skokie, IL, USA, 1961.
12. ACI-ASCE Committee 426. The Shear Strength of Reinforced Concrete Members. Chapter 5, Shear Strength of Slabs. *Proc. ASCE J. Struct. Div.* **1974**, *100*, 1543–1591. [CrossRef]
13. Mast, P.E. Stresses in Flat Plates Near Columns. *J. Proc.* **1970**, *67*, 761–768.
14. The International Federation for Structural Concrete. *fib Bulleting 2. Textbook on Behavior, Design and Performance Updated Knowledge of the CEB/FIP Model Code 1990*; fib: Lausanne, Switzerland, 1999; Volume 2. [CrossRef]

15. Muttoni, A. Punching Shear Strength of Reinforced Concrete Slabs without Transverse Reinforcement. *ACI Struct. J.* **2008**, *105*, 440–450.

16. Fernández Ruiz, M.; Muttoni, A. Application of Critical Shear Crack Theory to Punching of Reinforced Concrete Slabs with Transverse Reinforcement. *ACI Struct. J.* **2009**, *106*, 485–494.

17. Albuquerque, N.G.B.; Melo, G.S.; Vollum, R.L. Punching Shear Strength of Flat Slab-Edge Column Connections with Outward Eccentricity of Loading. *ACI Struct. J.* **2016**, *113*, 1117–1129. [CrossRef]

18. Hammil, N.; Ghali, A. Punching Shear Resistance of Corner Slab-Column Connections. *ACI Struct. J.* **1994**, *91*, 697–707. [CrossRef]

19. Narayani, N. Shear Reinforcement in Reinforced Concrete Column Heads. Ph.D. Thesis, Faculty of Engineering, Imperial College of Science and Technology, London, UK, 1971.

20. Zaghlool, E.E.-D.R.F. Strength and Behaviour of Corner and Edge Column-Slab Connections in Reinforced Concrete Flat Plates. Ph.D. Thesis, University of Calgary, Calgary, AB, Canada, 1971.

21. Anis, N.N. Shear Strength of Reinforced Concrete Flat Slabs without Shear Reinforcement. Ph.D. Thesis, Imperial College London, London, UK, 1970.

22. Hanson, N.W.; Hanson, J.M. Shear and Moment Transfer between Concrete Slabs and Columns. *J. PCA Res. Dev. Lab.* **1968**, *11*, 2–16. Available online: https://www.concrete.org/publications/internationalconcreteabstractsportal/m/details/id/19463 (accessed on 3 April 2022).

23. Stamenkovic, A. Local Strength of Flat Slabs At Column Heads. Ph.D. Thesis, Imperial College London, London, UK, 1970.

24. De Pina Ferreira, M.; Oliveira, M.H.; Melo, G.S.S.A. Tests on the punching resistance of flat slabs with unbalanced moments. *Eng. Struct.* **2019**, *196*, 109311. [CrossRef]

25. Ritchie, M.; Ghali, A.; Dilger, W.; Gayed, R.B. Unbalanced Moment Resistance by shear in Slab-Column Connections: Experimental Assessment. *ACI Struct. J.* **2006**, *103*, 74–82.

26. Sudarsana, I.K. Punching Shear in Edge and Corner Column Slab Connections of Flat Plate Structures. Ph.D. Thesis, Department of Civil Engineering, University of Ottawa, Ottawa, ON, Cananda, December 2001.

27. Zaghloul, A. Punching Shear Strength of Interior and Edge Column-Slab Connections in CFRP Reinforced Flat Plate Structures Transferring Shear and Moment. Ph.D. Thesis, Department of Civil and Environmental Engineering, University of Ottawa, Ottawa, ON, Canada, February 2007.

28. Desayi, P.; Seshadri, H.K. Punching shear strength of flat slab corner column connections. In *Part 1. Reinforced Concrete Connections*; Department of Civil Engineering, Indian Institute of Science: Bangalore, India, 1997.

29. Walker, P.R.; Regan, P.E. Corner column-slab connections in concrete flat plates. *ASCE J. Struct. Eng.* **1987**, *113*, 704–720. [CrossRef]

30. Stamenkovic, A.; Chapman, J.C. Local strength at column heads in flat slabs subjected to a combines vertical and horizontal loading. *Proc. ICE* **1974**, *57*, 205–232.

31. Vargas, D.; Lantsoght, E.; Genikomsou, K. *Spreadsheet for Flat Slabs in Eccentric Punching Shear: Experimental Database and Analysis*; Zenodo: Quito, Ecuador, 2022. [CrossRef]

32. Sarveghadi, M.; Gandomi, A.H.; Bolandi, H.; Alavi, A.H. Development of prediction models for shear strength of SFRCB using a machine learning approach. *Neural Comput. Appl.* **2019**, *31*, 2085–2094. [CrossRef]

33. Nemetschek Group. SCIA Downloads. 17 May 2022. Available online: https://www.scia.net/en/scia-engineer/downloads (accessed on 3 April 2022).

34. Lantsoght, E. Database of Shear Experiments on Steel Fiber Reinforced Concrete Beams without Stirrups. *Materials* **2019**, *12*, 917. [CrossRef] [PubMed]

35. Vargas, D.; Lantsoght, E.; Genikomsou, K. *Spreadsheet Validation for Flat slabs in Eccentric Punching Shear Experimental Database and Analysis*; Zenodo: Quito, Ecuador, 2022. [CrossRef]

36. Ngo, T. Punching shear resistance of high-strength concrete slabs. *Electron. J. Struct. Eng.* **2001**, *1*, 52–59. Available online: https://ejsei.com/EJSE/article/view/14 (accessed on 3 April 2022). [CrossRef]

37. Guandallini, S.; Burdet, O.L.; Muttoni, A. Punching Tests of Slabs with Low Reinforcement Ratios. *ACI Struct. J.* **2009**, *106*, 87–95.

38. Carrera, B.; Lantsoght, E.O.L.; Alexander, S.D.B. *Application of Strip Model to Edge Column-Lab Connections Loaded with Outward Eccentricity*; ACI: Farmington Hills, MI, USA, 2022; Volume 353, pp. 124–141. Available online: https://www.concrete.org/publications/internationalconcreteabstractsportal.aspx?m=details&id=51737115 (accessed on 3 April 2022).